TKK Dissertations 50
Espoo 2006

HIGH-ACCURACY CHARACTERIZATION OF OPTICAL COMPONENTS: DETECTORS, COATINGS AND FIBERS

Doctoral Dissertation

Antti Lamminpää

Helsinki University of Technology
Department of Electrical and Communications Engineering
Metrology Research Institute

TKK Dissertations 50
Espoo 2006

HIGH-ACCURACY CHARACTERIZATION OF OPTICAL COMPONENTS: DETECTORS, COATINGS AND FIBERS

Doctoral Dissertation

Antti Lamminpää

Dissertation for the degree of Doctor of Science in Technology to be presented with due permission of the Department of Electrical and Communications Engineering for public examination and debate in Auditorium S4 at Helsinki University of Technology (Espoo, Finland) on the 1st of December, 2006, at 12 noon.

Helsinki University of Technology
Department of Electrical and Communications Engineering
Metrology Research Institute

Teknillinen korkeakoulu
Sähkö- ja tietoliikennetekniikan osasto
MIKES TKK Mittaustekniikka

Distribution:
Helsinki University of Technology
Department of Electrical and Communications Engineering
Metrology Research Institute
P.O. Box 3000
FI - 02015 TKK
FINLAND
URL: http://metrology.tkk.fi/
Tel. +358-9-4511
Fax. +358-9-451 2222
E-mail: antti.lamminpaa@tkk.fi

© 2006 Antti Lamminpää

ISBN-13 978-951-22-8480-1
ISBN-10 951-22-8480-4
ISBN-13 978-951-22-8481-8 (PDF)
ISBN-10 951-22-8481-2 (PDF)
ISSN 1795-2239
ISSN 1795-4584 (PDF)
URL: http://lib.tkk.fi/Diss/2006/isbn9512284812/

TKK-DISS-2213

Otamedia Oy
Espoo 2006

HELSINKI UNIVERSITY OF TECHNOLOGY
P. O. BOX 1000, FI-02015 TKK
http://www.tkk.fi

ABSTRACT OF DOCTORAL DISSERTATION

Author Antti Jeremias Lamminpää

Name of the dissertation

High-accuracy characterization of optical components: detectors, coatings and fibers

Date of manuscript 10.8.2006	Date of the dissertation 1.12.2006
☐ Monograph	☒ Article dissertation (summary + original articles)

Department	Electrical and Communications Engineering
Laboratory	Metrology Research Institute
Field of research	Measurement Science and Technology
Opponent	Dr. Pedro Corredera Guillén
Supervisor	Prof. Erkki Ikonen

Abstract

The work described in this thesis is concentrating on the high-accuracy characterization of optical components.

Two trap detectors utilizing germanium and GaAsP photodiodes are constructed and characterized. The results for germanium detectors show that trap detector is well-suitable for applications where harmful inter-reflections need to be avoided. Furthermore, the spatial uniformities of the germanium photodiodes have improved significantly during the recent years. However, germanium detectors have relatively low shunt resistance, which needs to be taken into account when high-accuracy measurements are carried out. Unlike silicon detectors, the GaAsP detectors offer smooth spectral responsivity in the ultraviolet wavelength region and solar blindness. In addition the trap configuration approximately doubles, otherwise relatively low, spectral responsivity of the GaAsP photodiodes. The responsivity of both studied trap detectors is traceable to the cryogenic radiometer making them suitable for absolute power calibrations.

The reliability of the optical characterization methods relies strongly on the accuracy and properties of the applied detectors. High precision spectrophotometric measurements performed at various oblique angles of incidence can improve the determination of optical parameters of thin films. However, this requires systematic error factors such as misalignment in polarization plane and incidence angle and quality of beam collimation to be taken into account. The spectral reflectance and transmittance measurements are carried out for incidence angles varying between normal and Brewster's angle and the results are compared. For the first time, the reached consistency of ~ 0.2 % between the results confirms the accuracy of the spectrophotometric characterization technique.

The determination of nonlinearity of optical fibers has become more important as the transmission lengths and used optical power has increased in optical long-haul networks. In the thesis, two major improvements for the continuous-wave self-phase modulation method for the determination of nonlinear coefficient of optical fibers have been demonstrated. The first one is a technique to take the effects of dispersion into account by using mathematical modeling based on the Nonlinear Schrödinger Equation. Another one is a measurement scheme of high fiber optic power based on the integrating sphere detector. Together these improvements reduce the uncertainty in the determination of nonlinear coefficient to the level of 2.0 % (k = 2).

Keywords: measurement standard, thin films, spectrophotometry, nonlinear fiber optics, ultraviolet, infrared

ISBN (printed)	951-22-8480-4	ISSN (printed)	1795-2239
ISBN (pdf)	951-22-8481-2	ISSN (pdf)	1795-4584
ISBN (others)		Number of pages	57 p. + app. 34 p.

Publisher Helsinki University of Technology, Metrology Research Institute

Print distribution Helsinki University of Technology, Metrology Research Institute

☒ The dissertation can be read at http://lib.tkk.fi/Diss/2006/isbn9512284812/

TEKNILLINEN KORKEAKOULU PL 1000, 02015 TKK http://www.tkk.fi	VÄITÖSKIRJAN TIIVISTELMÄ
Tekijä Antti Jeremias Lamminpää	
Väitöskirjan nimi Valoilmaisimien, ohutkalvojen ja valokuitujen tarkkuuskarakterisointi	
Käsikirjoituksen jättämispäivämäärä 10.8.2006	Väitöstilaisuuden ajankohta 1.12.2006
☐ Monografia	☒ Yhdistelmäväitöskirja (yhteenveto + erillisartikkelit)
Osasto Sähkö- ja tietoliikennetekniikan osasto Laboratorio MIKES TKK Mittaustekniikka Tutkimusala Mittaustekniikka Vastaväittäjä Dr. Pedro Corredera Guillén Työn valvoja Prof. Erkki Ikonen	

Tiivistelmä

Väitöskirjassa esitellään germanium- ja GaAsP- pohjaisten valoilmaisimen karakterisointiprosessi. Molemmat ilmaisimet on toteutettu niin kutsuttua loukkuilmaisintekniikkaa käyttäen, mikä vähentää takaisinheijastusten määrää verrattuna yksittäiseen valodiodiin. Tehty tutkimus osoittaa, että etenkin suuripinta-alaisten germanium-valodiodien paikkavasteen tasaisuus on parantunut selvästi viime vuosien aikana. Vaikka germanium soveltuukin käytettäväksi tarkoissa lähi-infrapuna-alueen mittauksissa, täytyy sen suhteellisen alhainen rinnakkaisvastus ottaa huomioon valittaessa sopivaa transimpedanssivahvistinta. GaAsP-valodiodien käyttö loukkuilmaisinrakenteena nostaa valodiodien melko alhaisen spektrisen herkkyyden kaksinkertaiseksi. Lisäksi GaAsP-valoilmaisimilla on kaksi merkittävää etua yleisesti käytettyihin pii-pohjaisiin ilmaisimiin verrattuna. GaAsP-valodiodien spektrinen herkkyys on tasainen ultraviolettialueella ja niiden herkkyys rajoittuu näkyvälle valolle tehden niistä sokeita infrapuna-alueen valolle.

Tarkkoja valon spektrimittauksia voidaan hyödyntää myös ohutkalvojen optisten ominaisuuksien kartoittamisessa. Työssä esitellään tekniikka, jossa näytteelle osuvan valon tulokulmaa muuttamalla voidaan parantaa ohutkalvojen taitekertoimen ja paksuuden määrittämisen luotettavuutta. Näiden eri kulmissa suoritettujen heijastus- ja läpäisymittausten tulokset ovat yhteneviä ~ 0,2 % tarkkuudella. Väitöskirjassa esitetyt tulokset osoittavatkin, että huomioimalla ja poistamalla systemaattisten virhelähteiden vaikutus voidaan ohutkalvojen karakterisoinnissa saavuttaa erittäin tarkkoja tuloksia. Tulosten yhdenmukaisuus myös varmentaa ensi kertaa spektrofotometrisen menetelmän luotettavuuden optisten ohutkalvojen karakterisoinnissa.

Tiedonsiirrossa on tärkeää pystyä ennalta arvioimaan siirtotien vaikutus siirrettävään signaaliin. Käytettäessä suuria optisia tehoja alkavat niin kutsutut epälineaariset ilmiöt vääristämään valokuidussa etenevää signaalia. Tämän takia olemme kehittäneet parannuksia mittausmenetelmään, joka hyödyntää kaksitaajuisen signaalin kokemaa itseisvaihemodulaatiota valokuidun epälineaarisuuden määrittämisessä. Väitöskirjassa esitetään helposti käyttöönotettava tekniikka, jonka avulla voidaan ottaa huomioon kuitudispersion vaikutus epälineaarisuusmittauksen tuloksiin. Työssä on myös toteutettu mittausjärjestely, jolla voidaan pienentää tehomittauksesta syntyvä epävarmuuskomponentti 1,5 %:iin. Näiden parannusten ansiosta valokuidun epälinaarisuus n_2/A_{eff} voidaan määrittää aiempaa selvästi luotettavammin 2 %:n (k = 2) tarkkuudella.

Asiasanat mittanormaali, ohutkalvot, spektrofotometria, epälineaarinen kuituoptiikka, ultravioletti, infrapuna	
ISBN (painettu) 951-22-8480-4	ISSN (painettu) 1795-2239
ISBN (pdf) 951-22-8481-2	ISSN (pdf) 1795-4584
ISBN (muut)	Sivumäärä 57 s. + liit. 43 s.
Julkaisija Teknillinen korkeakoulu, MIKES TKK Mittaustekniikka	
Painetun väitöskirjan jakelu Teknillinen korkeakoulu, MIKES TKK Mittaustekniikka	
☒ Luettavissa verkossa osoitteessa http://lib.tkk.fi/Diss/2006/isbn9512284812/	

Preface

The research work described in this thesis has been carried out at the Metrology Research Institute, Department of Electrical and Communications Engineering of the Helsinki University of Technology, during the years 2003 – 2006.

I wish to thank Professor Pekka Wallin, the head of the Department, for providing me the opportunity to conduct scientific research on this interesting field of optical metrology.

I am most grateful to my supervisor, Professor Erkki Ikonen, for his guidance, encouragement and support during these years.

My special thanks go to Dr. Farshid Manoocheri for sharing his knowledge in the field of optics. Your advices throughout these years have been the most valuable.

I would like to thank my co-authors and colleagues at the Metrology Research Institute. Especially Dr. Tapio Niemi, Dr. Petri Kärhä, Dr. Hanne Ludvigsen, Dr. Saulius Nevas, Dr. Mart Noorma, Dr. Jouni Envall, M.Sc. Tuomas Hieta, M.Sc. Tuomas Hyyppä, Seppo Metsälä and Dr. Markku Vainio. Your contribution to the scientific and sometimes also to the non-scientific atmosphere of the laboratory has been undisputable.

The preliminary examiners of the thesis, Professor Martti Kauranen and Associate Professor Per-Olof Hedekvist, are highly appreciated for their efforts.

The financial support by the Finnish Cultural Foundation and Graduate School of Electrical and Communications Engineering is greatly appreciated.

Finally, I want to express my sincere gratitude to my fiancée Gerd and my parents for their love and support during my studies and the writing of the thesis.

Espoo, November 2006

Antti Lamminpää

List of publications

This thesis consists of an overview and the following selection of the author's publications.

[P1] A. Lamminpää, M. Noorma, T. Hyyppä, F. Manoocheri, P. Kärhä and E. Ikonen, "Characterization of germanium photodiodes and trap detector", *Meas. Sci. Technol.* **17**, 908-912 (2006).

[P2] M. Noorma, P. Kärhä, A. Lamminpää, S. Nevas and E. Ikonen, "Characterization of GaAsP trap detector for radiometric measurements in ultraviolet wavelength region", *Rev. Sci. Instrum.* **76**, 033110 (2005).

[P3] A. Lamminpää, S. Nevas, F. Manoocheri and E. Ikonen, "Characterization of thin films based on reflectance and transmittance measurements at oblique angles of incidence", *Appl. Opt.* **45**, 1392-1396 (2005).

[P4] A. Lamminpää, T. Niemi, E. Ikonen, P. Marttila and H. Ludvigsen, "Effects of dispersion on nonlinearity measurement of optical fibers", *Opt. Fiber Technol.* **11**, 278-285 (2005).

[P5] A. Lamminpää, T. Hieta, J. Envall and E. Ikonen, "Reliable determination of optical fiber nonlinearity using dispersion simulations and improved power measurements", *accepted for publication in J. Lightwave Technol.* (2006).

Author’s contribution

The scientific work presented in the thesis has been carried out at the Metrology Research Institute during the years 2003-2006. The thesis consists of a short overview and five publications referred as [P1-P5]. All publications are results of team work of the contributing scientists. The author has written papers [P1, P3-P5], and contributed to the writing of [P2].

The author did perform or coordinate all the experimental work presented in [P1]. He also took part in the construction of detectors described in the publication and was responsible for all the data analysis.

The spectral reflectance measurements in [P2] were performed by the author. He has also contributed to the analysis of the properties of the constructed detector.

The author has performed all measurements in the near-infrared and repeated part of the measurements in the visible wavelength region in [P3]. He has also carried out the analysis of the measurement results.

The author contributed to the planning of the research described in [P4] and he performed all the measurements and data analysis. Based on the results, reported in [P4], he initiated the research of [P5]. In the latter study, he has been coordinating the performed measurements. He has also taken part to the preparation of the simulation software and has been responsible for the results of the project.

Table of contents

Preface 7

List of publications 8

Author's contribution 9

Table of contents 10

1 Introduction 11

1.1 Background 11

1.2 Progress in this work 12

2 Optical detectors 14

2.1 Scale realization of spectral responsivity and spectral irradiance 14

2.2 Trap detector configuration 15

2.3 Germanium trap detector for near infrared wavelength region 17

2.4 GaAsP trap detector for ultraviolet wavelength region 20

2.5 Integrating sphere detector for measurements at fiber optic wavelengths 24

3 Optical coatings 28

3.1 Optical thin film structures 28

3.2 Spectrophotometric characterization methods for thin films 29

3.3 Characterization of optical thin films in various angles of incidence 31

4 Measurement of optical fiber nonlinearity 34

4.1 Nonlinear refractive index 34

4.2 Nonlinear light propagation in optical fibers 35

4.3 Continuous-wave self-phase modulation method 37

4.4 Effects of dispersion 42

4.5 Measurement of high fiber optic power 45

4.6 Uncertainty analysis 46

5 Conclusions 48

References 50

1 Introduction

1.1 Background

The possibilities of novel optical technologies are often limited by the accuracy to characterize their design parameters. To fine-tune the manufacturing processes of state-of-the-art devices, or even mass product articles, high-accuracy characterization methods are needed. Despite the constant improvements in precision and versatility of the characterization methods, the accuracy in optical measurement technology has remained one of the least reliable of all physical measurements [1]. Under ideal laboratory conditions, experts are able to carry out measurements, where relative uncertainty values are in the region of a few tenths of percent. Some quantities set higher limitations for measurement error and their uncertainties can remain at the level of few percents. However, this is just the case of laboratory work as in many practical situations measurement errors of 10 percent are commonplace.

The reliability of the optical characterization methods relies strongly on the accuracy and properties of the applied detectors. Today the high precision optical metrology is based on the accuracy of the cryogenic absolute radiometer [2], which as a primary standard links the optical quantities to the definition of electrical units and therefore to the international system (SI) of units. Among the other national metrology institutes (NMIs) around the world, Helsinki University of Technology (TKK) has established its spectral power responsivity scale on the cryogenic radiometer [3, 4, 5 6, 7, 8, 9, 10, 11]. In order to transfer the accuracy of the cryogenic radiometers to more practical transfer standard detectors, so called trap detectors [12, 13] have gained popularity. Trap detector is a construction of several photodiodes aligned to trap the light effectively inside the structure. At first, only silicon (Si) photodiodes were used in the trap detectors, but the need to extend the measurement capabilities to ultraviolet and near-infrared wavelength regions has introduced new trap detectors taking advantage of semiconductor materials such as gallium arsenide phosphide (GaAsP) [P2, 14], platinum silicide (PtSi) [15, 16], germanium (Ge) [17, P1] and indium gallium arsenide (InGaAs) [18].

Spectrophotometry is a field of science, where the power of optical radiation is measured in narrow wavelength intervals. These measurements can be used to quantify optical properties of materials and artifacts by determining their reflection, transmission or absorption of light waves. One interesting application for high-accuracy spectrophotometric measurements lies in the characterization of optical coatings. By defining the optical properties, such as the complex index of refraction and the layer thickness, more accurately, we can characterize and further improve the design and construction of the various optical devices, such as highly reflecting mirrors or antireflection coated optics that use thin-film layer structures.

Optics has always been inspired by its possibilities of making decorative and colorful demonstrations. The same reason inspired the early glass fiber drawing of fine narrow fibers, until their potentiality in optical data transmission was understood [19]. This was followed by two major inventions: all-optical amplifier [20, 21] in late 1980s and wavelength division multiplexing (WDM) [22, 23] more than ten years earlier. Together they gave a major impact on the incredibly fast growth of telecommunication capabilities.

Today the fiber optic networks have spread to almost everywhere. The ever-growing need of higher transmission rates with lower costs has increased the number of channels and thus the amount of power launched into the single optical fiber. This development has caused the nonlinear properties of optical fibers to start to appear [24, 25].

The nonlinear phenomena arise when high optical power is used to transmit the optical signal through the fiber path [26]. Therefore, the nonlinear coefficient of optical fibers n_2/A_{eff} has become one of the key parameters in defining the modern optical transmission fiber. It contains the effective area of optical fiber A_{eff}, which takes into account the fact that the magnitude of nonlinear effects depends on the axial power distribution inside the fiber, and the nonlinear refractive index n_2. Both parameters n_2 and n_2/A_{eff} can be used to present the intensity I or power P dependence of the refractive index of optical fibers n through a simple relation $n = n_0 + n_2 I = n_0 + (n_2/A_{\mathrm{eff}})P$, where n_0 presents the linear part of the refractive index [26]. The nonlinear coefficient of optical fibers n_2/A_{eff} may also have interesting applications in special fibers, such as doped fibers and photonic crystal fibers, where high optical powers can be used together with a great variety of dispersion and nonlinear properties.

Even though the applications of fiber optics are clearly different from those of free-space optics, several measurement techniques are practically the same. There are very little means to access the light propagating inside a waveguide, and eventually almost all measurements need to be performed outside the fiber. Finally, the same techniques of using optical gratings, integrating spheres and photodiodes prove to be useful in the wide field of fiber optics as in the spectrophotometry. However, to better understand fiber optics and phenomena that take place during the light propagation in optical fibers, some estimations and modeling are used. The simulations based on the wave theory [26], originating from Maxwell equations which describe the behavior of both the electric and magnetic fields, as well as their interactions with matter, can be used to model light propagation inside silica medium. Such an analysis with some knowledge of transmission waveguide properties can be used to isolate different phenomena and their effects on transmitted light. This gives us a powerful tool that in combination with optical measurement science and technology can further improve the understanding and characterization accuracy of optical components in fiber optics.

1.2 Progress in this work

The main goals of the research described in this thesis are development of detectors for spectrophotometric measurements and their applications in the characterization of optical thin films. Similar approaches are also exploited for the study of fiber parameters, where simulations and measurements are combined in order to achieve a high accuracy technique for the determination of fiber nonlinearity.

The first research topic of the thesis is covered in Chapter 2 where characterization of Ge [P1] and GaAsP [P2] trap detectors is briefly reviewed. The results for the Ge detectors show that the spatial uniformities of the large area photodiodes have improved significantly during the years. It is also possible to construct the Ge trap detector with very low reflectance of $\sim 10^{-4}$ in the near-infrared wavelength region making it well-suitable for applications where harmful interreflections need to be avoided. As a

drawback, Ge detectors have relatively low shunt resistance, which needs to be taken into account when high-accuracy measurements are carried out [P1]. The GaAsP trap detector is constructed and characterized for the first time in the work of [P2]. Unlike Si detectors, the GaAsP detectors offer smooth spectral responsivity in the ultraviolet wavelength region below 300 nm and solar blindness for wavelength above 700 nm. Furthermore the trap configuration approximately doubles the otherwise relatively low spectral responsivity of the GaAsP photodiodes. However, special attention needs to be paid for the amount of incident radiation to maintain the long-term stability of the detector [P2]. The responsivity of both studied trap detectors is traceable to the cryogenic radiometer making them suitable for absolute power calibrations.

Chapter 2.5 describes the work on the extension of the high fiber-optic power scale from 200 mW to 650 mW. The scale realization is based on an integrating sphere (ISP) detector having an InGaAs photodiode mounted on its exit port. The most important studied property is the linearity of power responsivity at high fiber-optic power levels. The extension of the power range of the ISP detector is required in the measurement of fiber nonlinearity, where high optical power is used to generate nonlinear effects [P5].

The reliability in the characterization of optical thin-film layer parameters greatly depends on the accuracy of spectrophotometric measurements. The confidence can be further improved, if the transmittance and reflectance measurements are performed at oblique angles of incidence, in addition to the normal incidence. However, systematic error factors such as accurate determination of the polarization plane, angle of incidence and quality of the beam collimation can become critical and need to be considered. In Chapter 3, measurements that satisfy these conditions have been carried out for a SiO_2 thin-film layer, and the analysis shows that the results are consistent with the high accuracy of 0.2 % [P3]. For the first time, consistency has been reached in the determined optical parameters of the thin-film layer obtained in oblique angles of transmittance and reflectance measurements. This remarkable achievement confirms the accuracy of the spectrophotometric characterization technique.

The traditional continuous-wave self-phase modulation (CW SPM) method to measure nonlinearity of optical fibers neglects the effects of fiber dispersion, which can cause systematic errors of several percents to the apparent results. This also limits the use of the method to only such conditions, where the dispersion effects are evaluated to be marginal. Unfortunately, such conditions are difficult to estimate a priori for the new type of fibers causing significant reliability problems for the CW SPM method [P4]. To overcome this problem, a new technique combining measurements and simulations using the Nonlinear Schrödinger Equation (NLSE) is introduced [P5]. To get the full benefit of the modeling of the light propagation, also the uncertainty related to determination of fiber-optic power needs to be brought to a satisfactory level. This is performed by using the integrating sphere detector described in Chapter 2.5.

2 Optical detectors

2.1 Scale realization of spectral responsivity and spectral irradiance

Traceability is a property of a measurement result, whereby it can be related to stated reference through a chain of comparisons all having stated uncertainties. This unbroken chain of comparisons is referred to as traceability chain. Optical detectors used for the scale realization of spectral power responsivity are all traceable to the absolute cryogenic radiometers [2] maintained by National Metrology Institutes. It is a primary standard for optical power measurements and links the optical radiation measurements to electrical quantities and therefore finally to the definition of SI units [27]. The traceability chain for spectral power responsivity is illustrated in Figure 1. The listed detector types at every stage of the traceability chain are examples of the instruments used at the TKK.

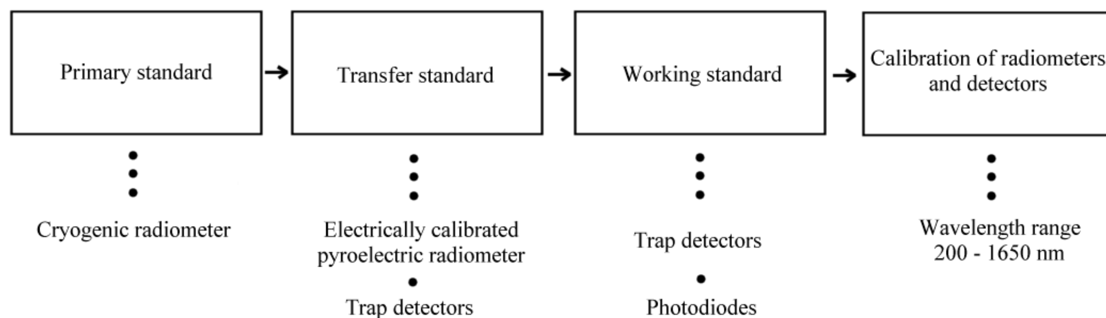

Figure 1. Traceable detectors are calibrated against instruments that are traceable to national or international standards. Primary standard [3] links the optical power measurements to the definition of SI units. Listed examples are selected among the instruments used at the TKK.

The application usually determines the detector of choice. As detectors are selected for the scale realization of spectral responsivity, special attention for the properties of the optical detectors needs to be paid. The level of precision decreases along the chain of traceability, as the uncertainty of the high level standards is inherited to lower levels. Therefore, primary and transfer standards are maintained by NMIs [28, 29, 30, 31, 32, 33] in order guarantee high scientific level of metrology. Working standard detectors are then calibrated against transfer standards and used for calibration of radiometers and detectors by NMIs and accredited research and calibration laboratories.

The TKK method for measuring absolute spectral irradiance is based on filter radiometers whose components are characterized separately and the modified Planck’s radiation law [34, 35]. The calibration of the filter radiometers is traceable to the absolute cryogenic radiometer via spectral responsivity scale, making the detectors crucial components of the filter radiometers. Absolutely calibrated filter radiometers, consisting of a precision aperture [36], exchangeable narrow band interference filters [37] and a trap detector, are used as transfer standards. The characterized filter radiometers will be used to measure

the spectral irradiance of quartz-halogen-tungsten lamps. A continuous model will interpolate the irradiance values between the discrete irradiance data. The model is then fitted to the measurement results with a recursive iteration process [35].

The International Bureau of Weights and Measures (BIPM) maintains Key Comparison Database (KCDB) for photometric and radiometric quantities among other areas of metrology. It covers the fields of photometry, fiber optics and properties of detectors, sources and materials. The accuracy of the scale realizations of photometric and radiometric quantities can be confirmed in comparison measurements carried out according to the Mutual Recognition Agreement (MRA) [38] among participating NMIs. As a result of the comparisons, the measurement uncertainties claimed by NMIs are verified. The Calibration and Measurement Capabilities (CMCs) declared by NMIs are then collected in Appendix C of the MRA maintained by BIPM [39].

2.2 Trap detector configuration

Today, trap detectors are widely used as reference standard detectors in the ultraviolet, visible and near infrared wavelength regions. The first trap configuration consisting of four silicon photodiodes was introduced by Zalewski and Duda in 1983 [12]. The idea behind their trap detector was to reduce the amount of back reflected light and thus to increase the external quantum efficiency. This was done by arranging four Si photodiodes in a configuration, where seven interreflections took place on the diode surfaces before light escaped from the trap detector. With this type of configuration nearly 100 % external quantum efficiencies were possible to achieve over relatively wide wavelength range from visible to near-infrared [12].

Eight years later Fox [13] modified the original trap configuration to be less polarization sensitive by arranging three photodiodes to lie in a three-dimensional configuration, in which the first two are at 45 degrees with respect to the incident light and the third one is at normal angle. Five interreflections take place inside the trap before the reflected light leaves the detector [13]. This construction, presented in Figure 2, is nowadays widely adopted among optical research institutes especially due to its insensitivity against polarization effects [40]. To this day, a large range of different photodiodes have been used to construct similar trap detectors for the ultraviolet [P2, 14], visible [12, 13], and infrared [17, 18, P1] wavelength regions, as is also shown in Figure 3.

Typically, the trap detectors have low reflectance and relatively high responsivity. However, not all photodiodes enable to take full advantage of the trap configuration due to the reasons such as protective layer absorption [P2] or effects of low shunt resistance [P1]. During the years, other geometries have also been proposed for trap detectors [41] and also so called transmission trap detectors with no back reflection have been designed [42, 43]. These variations have brought improvements only in some special cases and the three-dimensional reflection trap configuration has remained in many cases the best compromise between the performance, simplicity of construction and overall price.

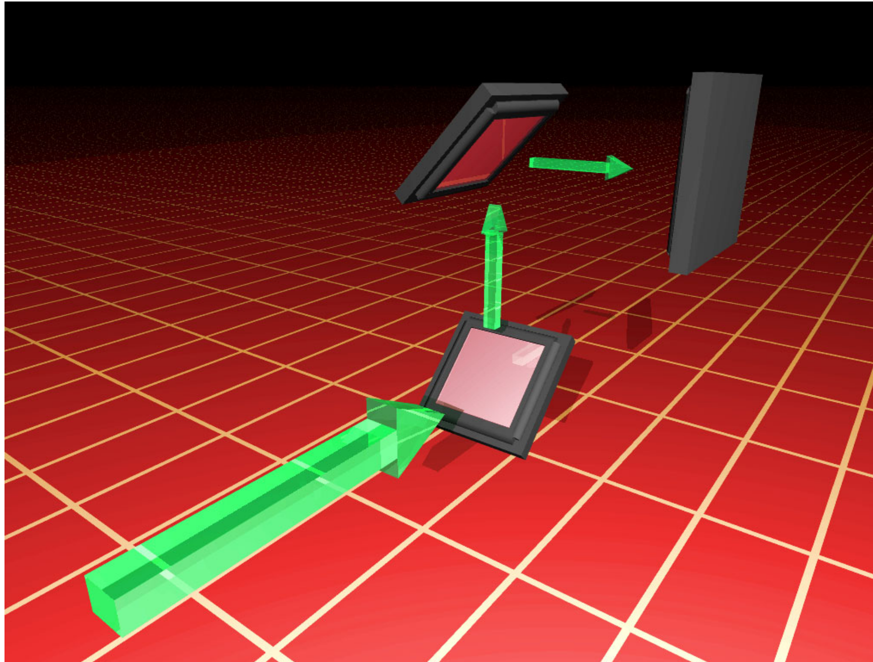

Figure 2. Layout of the photodiodes in a three-element reflection trap detector.

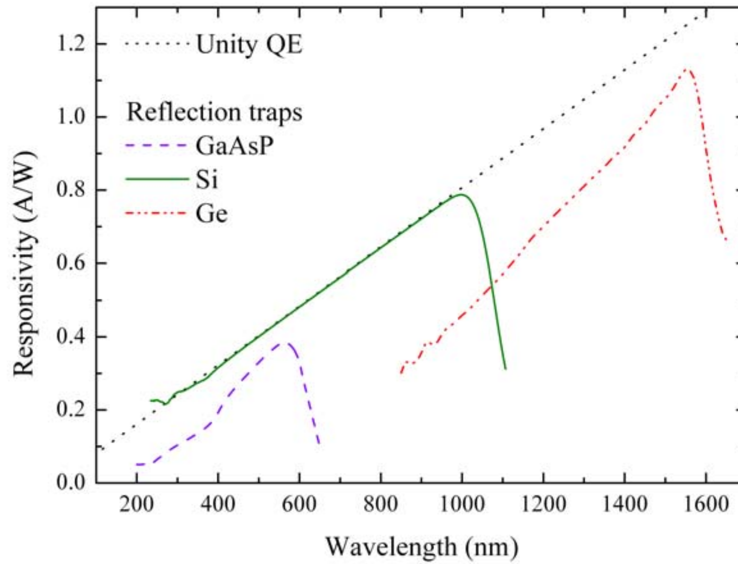

Figure 3. Spectral responsivities of GaAsP [P2], Si, and Ge [P1] trap detectors characterized at TKK. All detectors are currently used for calibration purposes covering the wavelength range between 200 nm to 1650 nm.

2.3 Germanium trap detector for near infrared wavelength region

The Ge technology dates back to 1950s when it was extensively studied for the transistors. This research made good quality crystals available for studies of the photoelectric and optical properties. Nowadays large area Ge photodiodes are commercially available at moderate prices contrary to InGaAs photodiodes of similar diameters. Therefore Ge photodiodes potentially offer a cost effective technique for accurate radiometric measurements in the near infrared wavelength region.

In order to extend the detector-based spectral irradiance scale [34, 35] of TKK to the near infrared wavelength region, a Ge photodiode and a trap detector consisting of three Ge photodiodes have been constructed and characterized [P1]. Both detectors are shown in Figure 4.

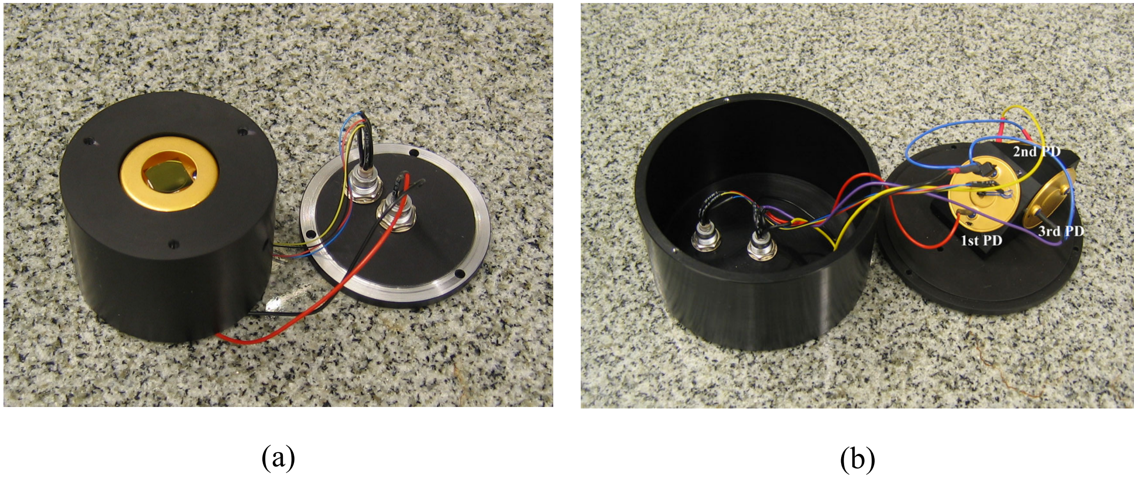

(a) (b)

Figure 4. (a) Ge photodiode mounted on a housing and (b) Ge trap detector body part, where photodiodes (PD) are indicated. The first two photodiodes are at 45 degrees angle with respect to the incident light and the third one is at normal incidence angle.

The spectral responsivity of large area Ge photodiodes in a trap detector configuration has been studied earlier by Stock *et al.* [17]. At TKK, the spectral responsivity measurements were carried out by using the monochromator-based reference spectrometer [44]. The spectral responsivity results for a Ge photodiode and the Ge trap detector are illustrated in Figure 5a. The spectral temperature coefficient of the Ge detectors was also studied and found to vary from -0.003/°C to 0.007/°C at the wavelength range of 850 nm to 1650 nm [P1] which is similar behavior as reported in earlier studies [17].

The spectral responsivity $R(\lambda)$ of a semiconductor detector can be expressed as [45]

$$R(\lambda) = [1 - \rho(\lambda)]\, \eta(\lambda)\, \frac{\lambda}{K}\,, \quad (1)$$

where λ is the vacuum wavelength of incident light, $\rho(\lambda)$ is the spectral reflectance of the detector, $\eta(\lambda)$ is the spectral internal quantum efficiency of the detector, and $K = hc / e = 1239.48$ nm W A^{-1} is determined in terms of fundamental constants.

The internal quantum efficiency (IQE) of Ge photodiodes was calculated from the measured spectral responsivity and the reflectance using Equation 1. The results presented in Figure 5b show that there are significant internal losses with the studied photodiodes. The absorption coefficient and the penetration depths with Ge photodiodes are strongly dependent on the wavelength. The long wavelength photons can penetrate deeper into the photodiode than shortwave photons, and therefore they are mainly absorbed in different volume elements of the detector [46, 47]. Since Ge has no native oxide that is well suitable as durable resistant passivation and antireflection coating, the concentration of recombination centers is much higher close to the interface between the Ge wafer and the passivation layer than at the Si-SiO_2 interfaces in the case of silicon detectors. Therefore, the decrease of IQE at short wavelengths is due to recombination at the interface of Ge-passivation layer and within the front region of the diode [48].

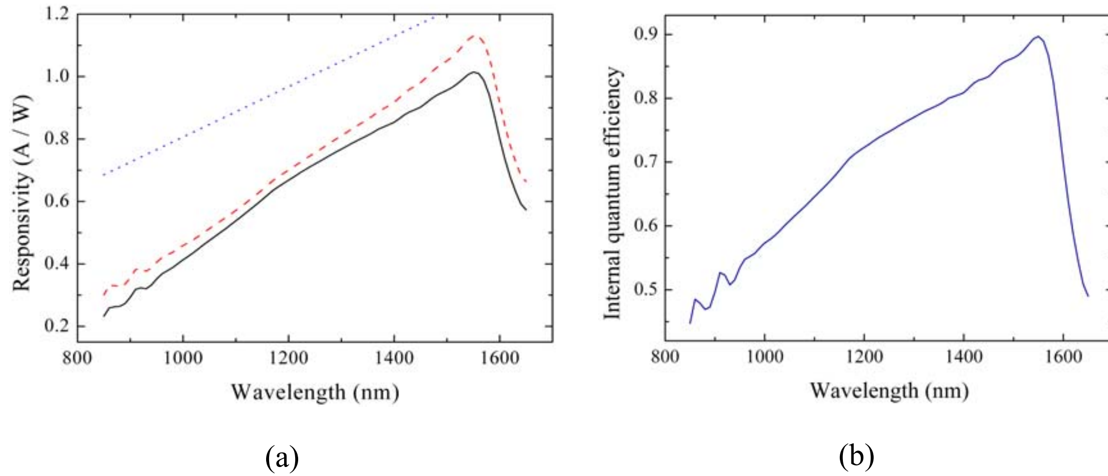

(a) (b)

Figure 5. (a) Spectal responsivity of Ge photodiode (solid black line) and Ge trap detector (dashed red line). The dotted blue curve shows unity quantum efficiency. (b) Internal quantum efficiency of the Ge detectors. [P1]

The internal losses can possibly have an effect on the long-term stability of the Ge photodiodes. Large area Ge photodiodes having even worse IQE have been studied, and their aging rate between 1100 nm and 1800 nm was found to be lower than ±0.5% per year [48]. Even though these results cannot be used to predict other diodes, they give an estimate for the severity of the aging effect. Another important issue to be considered is the radiation damage, which is not expected to take place at the wavelength region above 900 nm, where Ge photodiodes are normally used with moderate power levels of ~ 20 mW at the maximum. Earlier studies have shown that even the reversible fatigue effects with Ge photodiodes are negligible, if the diodes are radiated at wavelengths longer than 600 nm at power levels of a few microwatts [49].

The reflectances of the photodiodes were measured using the absolute gonioreflectometer programmed for specular reflectance measurements [50]. Additional comparison measurements were done with three different lasers. The results for a Ge photodiode are shown in Figure 6a. The reflectance of the Ge trap detector was then calculated based on the results of reflectance measurements of the individual Ge photodiodes, using equation

$$\rho_{\text{trap}} = \rho(0^\circ)\cdot\rho_s^2(45^\circ)\cdot\rho_p^2(45^\circ)\,, \qquad (2)$$

where $\rho(0°)$, $\rho_s(45°)$ and $\rho_p(45°)$ represent reflectance of the photodiodes at 0° and 45° for both polarization planes, respectively. The trap reflectance is needed, for instance, to make the inter-reflection correction when the components of filter radiometers are characterized separately. The calculated result was verified with a laser measurement at 1523 nm. The spectral reflectance of the Ge trap detector is plotted in Figure 6b.

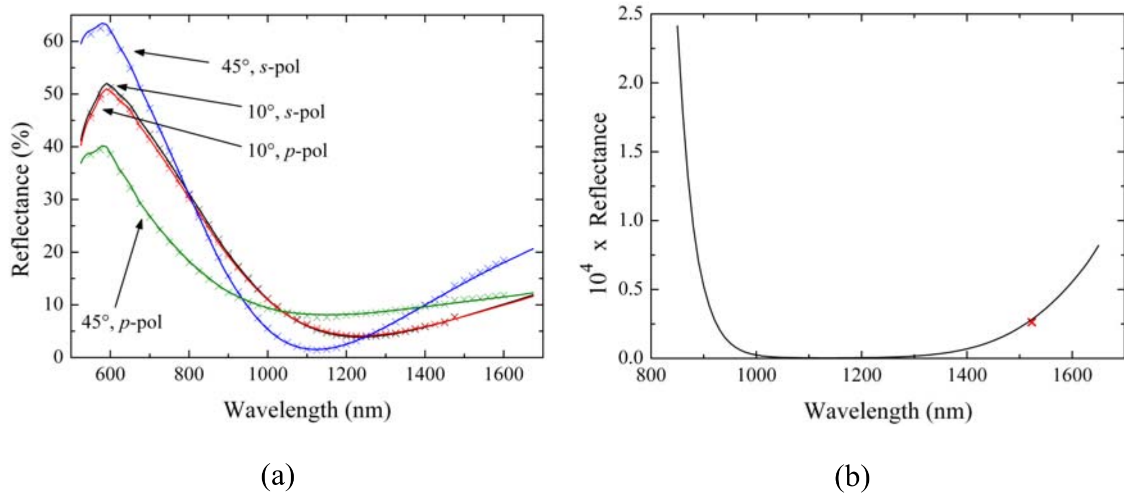

Figure 6. (a) Reflectance of the Ge photodiodes was measured at 10° and 45° incidence angles with both *s*- and *p*- polarized light. (b) Based on these results reflectance of the Ge trap was calculated and verified with a laser measurement at 1523 nm. [P1]

The studied Ge diodes have a thin film coating on top of the diode, which explains the shape of the spectral reflectance curves. In the analysis of thin film coating, the spectral reflectance measurements at oblique angles of incidence are combined with a mathematical model that considers a thin homogeneous layer of a dielectric material deposited on a macroscopically thick plane-parallel substrate [51, P3]. For the substrate characteristics, tabulated values for bare Ge [52] are used. The analysis reveals that the thicknesses of the thin film coatings of the four Ge photodiodes vary between 175 nm and 182 nm. As the refractive index is found to be at the level of ~ 1.7, the optical thickness of the thin film layer is approximately 300 nm, which makes it optimized for the wavelength region around 1200 nm. The analysis does not reveal any appreciable absorption in the thin film coating.

The current signals of the diodes are measured using current-to-voltage converters (CVC). When the gain setting of the CVC is adjusted, the input impedance of the device can change. Therefore, the relatively low shunt resistances of the Ge photodiodes (~ 5 kΩ) and trap detector (~ 1.7 kΩ) need to be taken into account. Otherwise, a significant ratio of the photocurrent can flow through the shunt resistance instead of the CVC. If the input impedance of the CVC increases from 1 Ω to 100 Ω, this can affect the apparent responsivity of the Ge photodiodes or of the trap detector by ~ 2 % or ~ 6 %, respectively.

Due to the low shunt resistance of Ge detectors, the detector and the amplifier should be constructed and characterized as one unit. One commonly used technique to increase the shunt resistance of the photodiode is the use of a bootstrap transimpedance amplifier [53]. Otherwise, Ge photodiodes demand for extra care, if used as transfer standards, as they should be calibrated for the different gain settings or the shunt and input impedances should be measured in order to be able to apply corrections. Even though the photodiodes have low shunt resistance, their noise level does not become a critical issue as the Johnson and dark current noises do not exceed the level of a few picoamperes.

The most severe drawback of the Ge photodiodes is their low shunt resistance and in turn significant dark current, which are both temperature dependent [54]. However, these problems can be reduced to a satisfactory level by either monitoring the detector temperature or by constructing temperature stabilization. In addition, our results show that the spatial uniformity of the Ge photodiodes has improved significantly over the years, when compared to earlier studies [55, 56], and is now at the level of ~ 0.1 % at the wavelengths of 1308 nm and 1550 nm [P1]. The reflectance of the Ge trap detector is found to be below the level of 10^{-4} in the near infrared wavelength region [P1]. This makes the Ge trap detector applicable for filter radiometry, such as spectral irradiance measurements, which are affected by inter-reflections between the detector and filter.

2.4 GaAsP trap detector for ultraviolet wavelength region

High accuracy radiometric measurements in the ultraviolet (UV) wavelength region of 200 - 400 nm set some special requirements for semiconductor photodiodes. These requirements include solar blindness, long-term stability of spectral properties, and stability of spectral responsivity under UV exposure. Use of silicon photodiodes is limited by the possible damage by high energy photons below 250 nm [57]. They also have high responsivity up to 1000 nm wavelength, which may cause severe leakage problems, if the detector is used for the filter radiometry in ultraviolet. Moreover, GaAsP photodiodes have smooth spectral responsivity at wavelengths below 300 nm unlike Si photodiodes. This is preferable as the responsivity is typically interpolated between measured values [58].

Gallium arsenide phosphide (GaAsP) Schottky-type photodiodes, which have cut-off wavelength around 610 nm, are widely used as working standard detectors in the UV wavelength region. The photodiodes are coated with a thin gold layer, which acts both as the Schottky contact and as a protection layer against oxidation. The GaAsP photodiodes meet to some extent most of the requirements listed earlier and they are commercially available with large active areas. Several research groups have investigated the properties

of GaAsP photodiodes [59, 60, 61, 62, 63, 64, 65, 66]. In addition to favorable properties, the research has revealed several problems. The responsivity of GaAsP photodiodes is usually 2 - 3 times lower as compared to Si photodiodes and the spectral responsivity changes rapidly under intense UV radiation [64]. In addition, the spatial uniformities of studied photodiodes have been modest [63, 64].

The properties of Au-GaAsP Schottky photodiodes in the trap detector configuration have been studied in order to extend the Finnish national scale of spectral responsivity, maintained at TKK, down to 200 nm [P2]. Photodiodes have been arranged in three-dimensional trap configuration [13] and they have been connected electrically in parallel.

The spectral responsivity of the GaAsP photodiode and trap detector were studied using a customized spectrophotometer, constructed and characterized at TKK [44]. The instrument is well-suitable for spectral responsivity measurements, because it is easily accessible for adjustments and systematic error components are controlled via careful characterization measurements. The measurement results are presented in Figure 7a. Also the internal quantum efficiencies (IQE) of the trap and of a single photodiode were calculated in the wavelength region between 250 and 400 nm using Equation 1. As clearly visible in Figure 7b, the comparison revealed a reduction of the apparent IQE of the trap detector as compared to the single photodiode at the level of ~ 10 %. The probable reason for this effect is the increased absorption in the Schottky contact layer of the photodiodes in the trap detector configuration, where two photodiodes are at 45° with respect to the incident light and thus the path length of the light through the contact layer is longer.

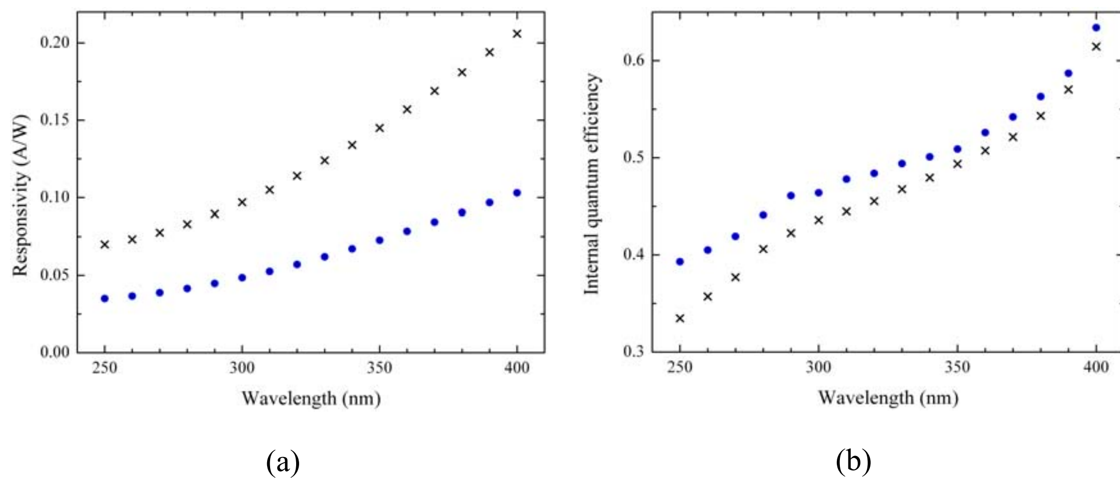

(a) (b)

Figure 7. (a) Trap configuration (black crosses) increases responsivity compared to the single GaAsP photodiodes (blue circles). (b) However, due to the absorption in the Schottky contact layer the IQE is lower when the trap configuration is used. [P2]

The high accuracy gonioreflectometer [50] was used to measure the spectral reflectance of a GaAsP photodiode in the wavelength range between 240 nm and 600 nm. The measurements were conducted at the angles of incidence of 45°, 30°, and 10° using linearly polarized light sequentially in *s*- and *p*-planes. The reflectance at the normal incidence was then calculated by extrapolation of the measured reflectances. The reflectance of GaAsP trap detector was calculated from the data using Equation 2. The results of the reflectance measurements are plotted in Figure 8. We also measured the reflectance of the trap detector as a whole at several laser wavelengths in order to verify the calculated reflectance. The measurements were conducted at 325 nm, 442 nm, and 457 nm. During the measurements, the trap detector was tilted 0.5° from the direction of the incident light in order to be able to measure the power of the reflected light. The relative deviations of the calculated reflectances of the trap detector from the measured values were around $5 \cdot 10^{-2}$ at all wavelengths. This corresponds approximately to the uncertainty of the measurements.

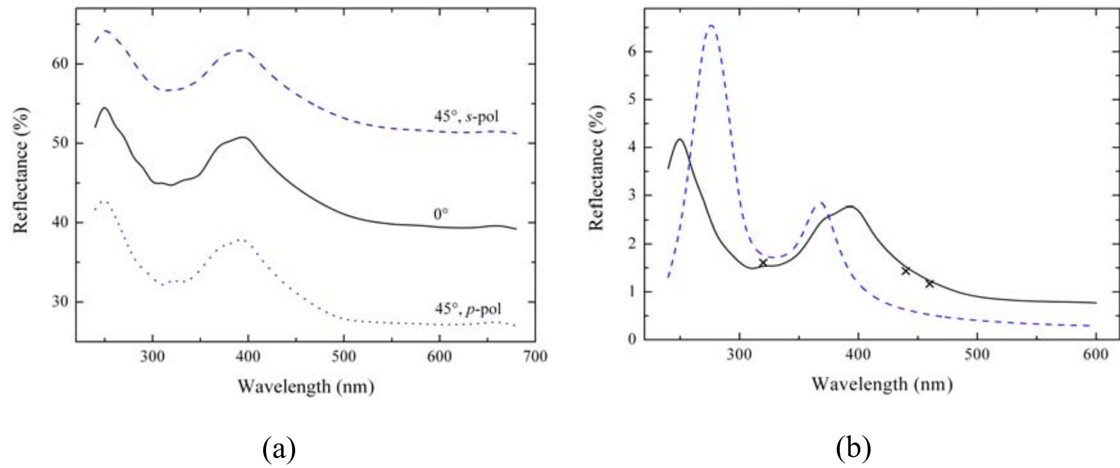

Figure 8. (a) GaAsP diode reflectance measured at 45° with both *s*- and *p*-polarizations. Reflectance at normal angle of incidence has been calculated based on the oblique angle measurements. (b) Based on these values the reflectance of the GaAsP trap (solid black line) has been calculated and compared with the reflectance of the Si trap detector (dashed blue line). The results for GaAsP trap reflectance have been verified with laser measurements at three different wavelengths (crosses). [P2]

The stability of the Au-GaAsP photodiodes was investigated during the characterization process under the conditions, where radiation doses and exposure times are equivalent to the actual applications of photodiodes. No systematic changes in spectral responsivity were detected during the measurements. It has also been demonstrated that the change of the responsivity of GaAsP Schottky photodiodes is slower compared to the corresponding change in the responsivity of a Si photodiode [62].

The spatial uniformity of the optical power responsivity was measured first separately for the single photodiodes. The measurements were carried out at two helium–cadmium laser wavelengths, 325 nm and 442 nm. The $1/e^2$ diameter of the laser beam was approximately 2 mm. One photodiode out of the four tested ones was rejected due to a

4 % responsivity peak near to its center. Typically, the responsivity was lowest in the center and increased close to the edges of the photodiodes by approximately 5 %. Next the trap detector was assembled, and the measurements were repeated with the trap detector. The measurements were conducted at the same laser wavelengths with similar diameters of the laser beam. The measured responsivities at 325 nm, relative to the responsivity at the center of the trap detector, are shown in Figure 9. On the average, the spatial uniformity of the assembled trap detector was approximately 2 times better as compared to that of the single photodiodes.

The accuracy of the alignment of the trap detector with the incident light beam is in the order of 0.5 mm for most of the measurement applications. From the measured spatial uniformities of the GaAsP trap detector at 325 nm and 442 nm wavelengths, the corresponding uncertainty contribution to the responsivity of the trap detector was calculated. In the case of a beam with 3 mm diameter, the relative standard uncertainty contribution is $4 \cdot 10^{-4}$ for both of the wavelengths. Due to the systematic increase of the responsivity towards the edges of the detector, it is necessary to apply a small correction to the responsivity of the trap detector if the beam sizes in the calibration and in the application are not equal. For example, the relative difference between the average responsivities of the trap detector for a 2 mm beam and for a 3 mm beam is $2 \cdot 10^{-4}$.

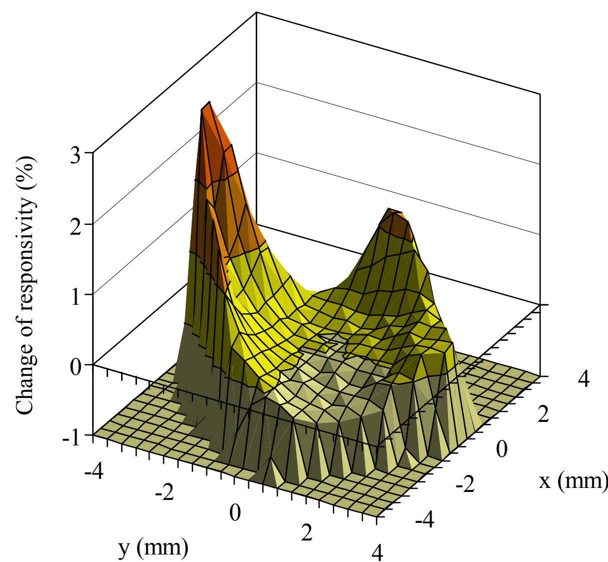

Figure 9. Spatial uniformity of GaAsP trap detector at 325 nm, measured using a 2 mm beam. [P2]

2.5 Integrating sphere detector for measurements at fiber optic wavelengths

Measurement of high fiber optic power has practical applications in optical amplifiers, fiber lasers and testing of long-haul telecommunication systems. The same power measurement principles can be exploited in the accurate determination of fiber nonlinearity. In the determination of fiber optic power, we are limited to measure either the optical power launched into the fiber or the power coupling out of the fiber. This is a fundamental measurement problem, when we are trying to determine the optical power inside a fiber system, as any modifications on the system would change the alignment of the fibers and interfere to the measurement conditions. To overcome this problem with satisfactory uncertainties, accurate methods to determine optical attenuation are needed. Commonly used cut-back method is one suitable alternative, as the measured fiber lengths are significantly longer as compared to the length of the lost fiber piece.

When the optical signal leaves the fiber, the light spreads into a relatively wide solid angle. This leads to problems with detector spatial uniformity and may therefore cause systematic errors. Systematic calibration errors of even 10 % have been recorded and the results have been varying depending on the connector type [67]. By taking this into account in the detector design, as low as ~ 0.1 % uncertainty contributions are possible due to the divergence of light from the fiber exit [68, 69]. Integrating sphere (ISP) detectors have been proposed for measurement of fiber optic power, as they have flat angular responsivity over wide solid angle [70, 71, 72, 73, 74]. Fortunately, the low throughput of the ISP detectors, which is normally considered as a downside, becomes an advantage as high fiber optic power is being measured. These types of detectors do not necessarily require use of any external attenuators in front of them to avoid the saturation of photodiode.

Part of the light is reflected backwards from the air-glass interface, as the light leaves the optical fiber [75]. This reflection has to be taken into account while we are determining the optical power inside the fiber by using detectors collecting exiting light [76, P5]. The reflected optical power can be determined with a measurement setup utilizing a 50:50 fiber coupler as illustrated in Figure 10. On the input side, a continuous laser source is connected into the first branch of the coupler and an optical detector into the second one. On the output side, first branch containing the FUT is connected directly to the ISP detector. It is now possible to see an interference effect to take place, on the optical detector located on the input side of the coupler, due to the small variations in optical path difference between two coupler branches. The magnitude of this interference effect depends on the conditions of the free output connector.

If both output fiber ends are in air, the reflected intensity at the optical detector varies between zero and a maximum value determined by the reflectance at the air-glass interface. When the free connector is dipped into water, having refractive index between air and SiO_2, the reflected intensity at optical detector does not reach the zero at any time. Finally, when refractive indices of the free connector and output medium are matched to prevent the back-reflection, the interference effect disappears and the total reflected light remains constant. It is now straightforward to calculate how much light is reflected on the connection between FUT and ISP [75]. These measurements showed that with studied SMFs the amount of back reflected light from the fiber end was 3.4 %.

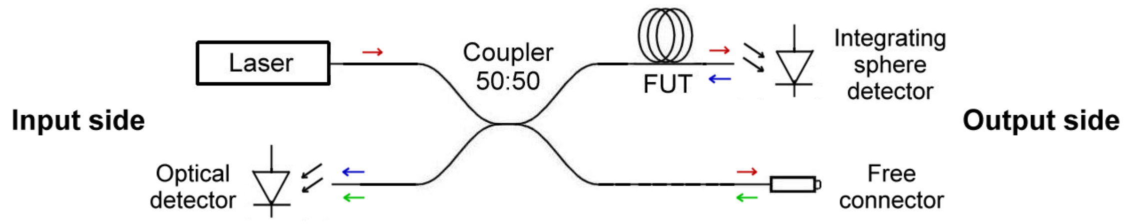

Figure 10. Measurement setup to determine reflection from the interface of FUT and air.

TKK maintains the scale of high fiber optic power at wavelength regions around 1.3 µm and 1.55 µm [72, 77]. The optical power region of this scale has been now extended to 650 mW [P5], which is the maximum output power of the used erbium-doped fiber amplifier (EDFA). The ISP detector designed for this purpose is presented in Figure 11. The ISP has two input ports on the equator of the sphere: the first one has a fiber connector for FC/PC and FC/APC connectors and the other one is an open port. An InGaAs photodiode of 5 mm diameter has been mounted on the exit port lying in the north pole of the sphere. The port 2, in Figure 11a, can be used in the characterization process of the sphere to map the linearity of power response and to measure the change in throughput when fiber adapter is attached.

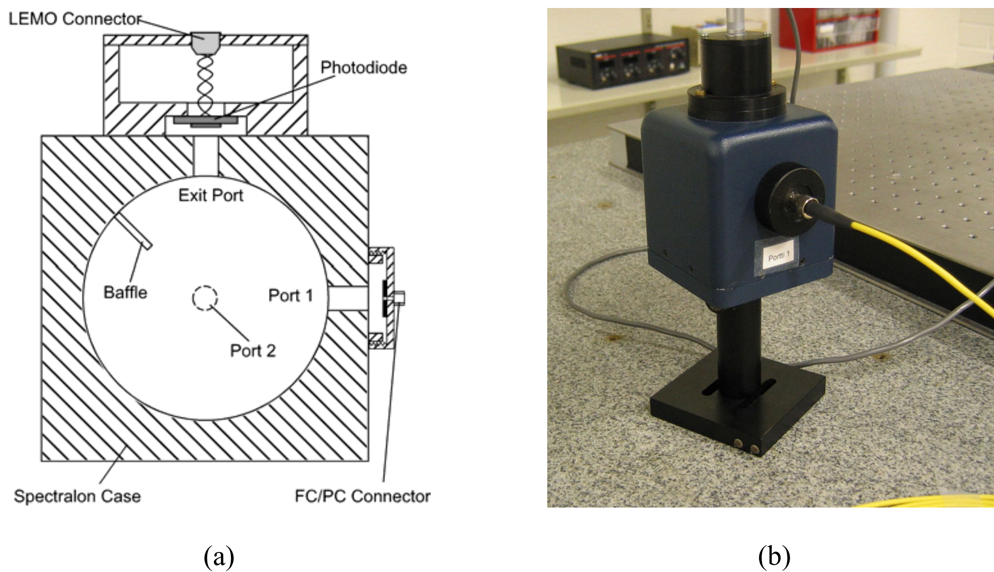

(a) (b)

Figure 11. (a) Schematic drawing [72] and (b) photograph of integrating sphere detector for high fiber optic power. Fiber connector input is located on port 1 lying on the equator of the sphere. InGaAs photodiode is mounted on the exit port on the north pole.

The diameter of the exit port is 4 mm and therefore the InGaAs photodiode mounted on it is over-illuminated. The linearity of the ISP detector was studied using the AC/DC method [78], where small intensity-modulated signal (AC) is accompanied with high intensity continuous wave signal (DC). The changes in AC light are then monitored with the help of a lock-in amplifier, as the DC level is increased. The results of the linearity measurement of the ISP detector response are presented in Figure 12. Especially when optical power of over 10 mW is measured with the detector, the nonlinear response of the detector needs to be taken into account. If a 1 mm aperture is placed in front of the InGaAs photodiode, the power response will be linear up to 650 mW as illustrated in Figure 13. This shows that the nonlinearity of the ISP detector is entirely a property of the used InGaAs photodiode. However the additional aperture was not taken into the use, as the sphere throughput and responsivity did drop significantly.

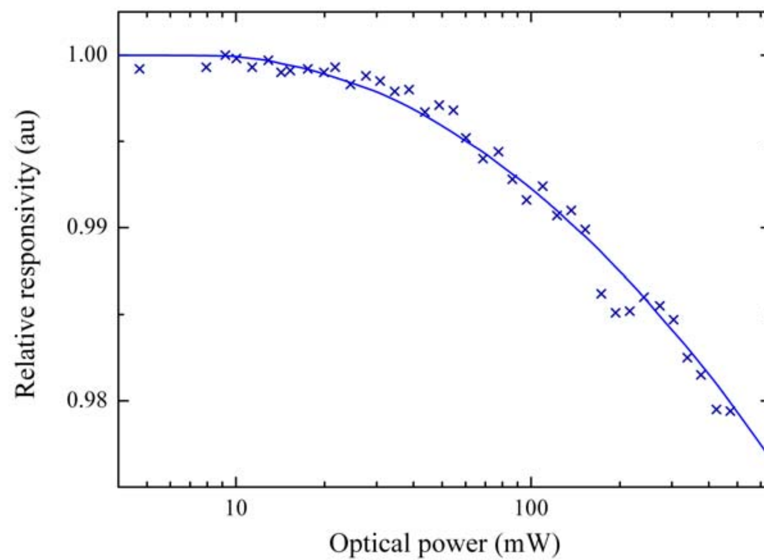

Figure 12. Linearity of the responsivity of the integrating sphere detector at 1550 nm wavelength. InGaAs photodiode is over-illuminated. [P5]

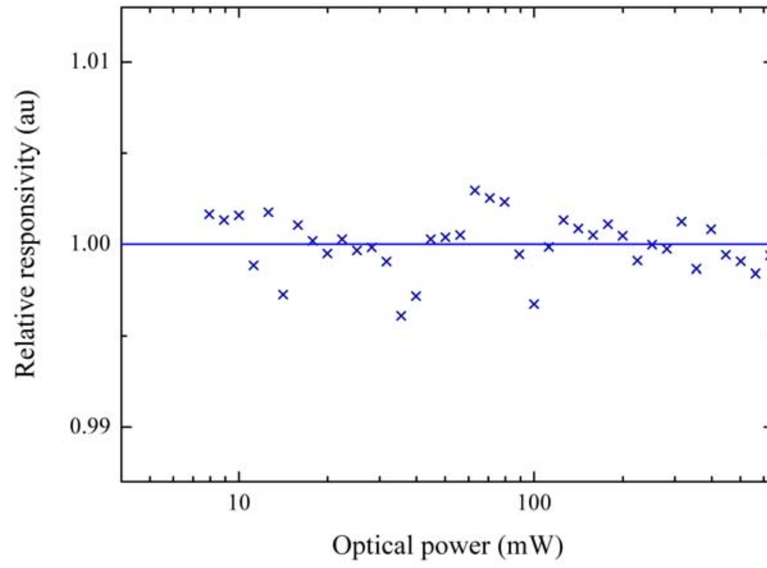

Figure 13. Linearity of the responsivity of the integrating sphere detector at 1550 nm wavelength. An aperture of 1 mm diameter is placed in front of the diode to prevent over-illumination conditions.

3 Optical coatings

3.1 Optical thin film structures

To understand why the application possibilities of optical thin film coatings are almost unlimited, we consider the interference effect that takes place in dielectric films. There is large variety of situations in which such interference can take place. Variables in the arrangement include the size and spectral width of the source and the shape and reflectance of the film. Figure 14 illustrates a practical simplification of the problem, where a beam of light is divided into a reflected and refracted portion at any boundary of the dielectric material. A condition called external reflection occurs with light going from lower index toward a higher index (e.g. $n_1<n_2$). On the other hand, when light is going from higher index medium to lower index medium, the effect called internal reflection takes place. A relative phase shift of 180° takes place between externally and internally reflected beams, so that equivalently, an additional path difference of $\lambda / 2$ is introduced between the two beams. If the optical thickness of thin film coating *d*, in Figure 14, is designed to match the wavelength $\lambda / 2$, the net optical path difference between the reflected beams is $\lambda + \lambda / 2$, which puts them precisely out of phase. This condition, called destructive interference, is opposite to the condition where reflected beams are in the same phase making the thin film coating a reflector. This condition is called constructive interference. [79]

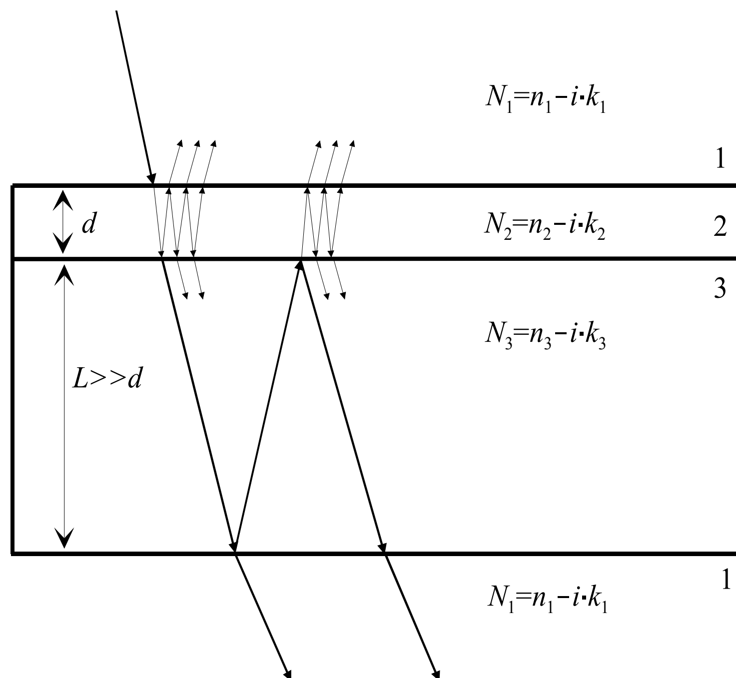

Figure 14. Interference effect takes place in thin film layer of thickness *d*. The substrate thickness *L* is orders of magnitude larger than *d* and the phases of the waves reflected from 3-1 interface are randomized relative to the waves reflected from interfaces 1-2 and 2-3.

For interference to occur between waves, they must be coherent. With laser light sources, the interference between waves can take place when the two waves' travel paths are quite different in length. White light from a thermal source on the other hand, does not have this coherence. In a typical thin film structure, where the total thickness of the stack is in the order of the wavelength, all the waves reflected from the interfaces can be added coherently. In this case, the amplitudes add, and the phases of the waves have to be taken into account when adding these amplitudes. The coherence length [80] of light is approximately

$$\Delta l = \frac{\lambda^2}{\Delta\lambda} , \quad (3)$$

where λ is the wavelength and $\Delta\lambda$ is the bandwidth.

For the continuous wave (CW) laser beam, the coherence length can be several meters and even for the picosecond lasers the coherence lengths can be in the order of hundreds of microns. In a monochromator that has a bandwidth of 1 nm, for example, Equation 3 leads to a coherence length of approximately 0.25 mm for the light with wavelength of 500 nm. A thin film layer of this thickness or thinner will produce the interference effect. When the length difference between two paths is greater than coherence length, the phases of two waves are randomized and they cannot interfere with each other. In such a situation, two waves behave as two incoherent sources. Such sources are combined by adding their intensities, rather than their complex amplitudes. [80]

The variety of different optical components that can be manufactured with thin film layer structures is enormous: narrow band-pass interference filters, highly reflective mirrors, antireflection-coated lenses, polarizers, WDM filters and gain-flattening filters for optical-fiber amplifiers are just a few examples. Thus the design of the these components is highly dependent on the knowing of optical parameters of deposited thin-film layers, the complex index of refraction and layer thickness need to be known accurately in order to achieve the optical properties of the components.

3.2 Spectrophotometric characterization methods for thin films

Optical properties of homogenous thin film layers are determined by the Maxwell equations by their complex index of refraction $N(\lambda) = n(\lambda) - ik(\lambda)$ and thickness of the layer d. The real part $n(\lambda)$ includes the normal dispersion and the extinction coefficient, $k(\lambda)$, governs the absorption of light waves propagating inside a medium. The transmission and reflection of light waves at the boundary of two media is also governed by the complex index of refraction. As presented in Figure 14, in a case of single dielectric film deposited on a macroscopically thick substrate, three interfaces will be formed. The reflection and transmission from these surfaces can be described using Fresnel complex amplitude coefficients [37, 81]. Both the reflected and transmitted waves are sums of multiple internal reflections at the three interfaces.

During the last decades there has been an enormous growth in the field of applications, where optical thin films are used. Because of this the research of different methods to

characterize optical thin films has increased remarkably. The variety of techniques is huge, and it is convenient to classify the methods to single-wavelength and multi-wavelength approaches based on the number of wavelengths used simultaneously for the characterization.

The single wavelength methods offer potentially accurate characterization results, but because of their single wavelength nature they are more vulnerable to both random and systematic errors in the measurements. Furthermore, the relation between optical parameters and the measured quantities is very complex. Therefore, the optical parameters are often derived through multiple successive iterations, which often lead to multiple solutions or no solution at all [51, 82]. Furthermore, even small measurement errors can cause the result to converge towards a wrong solution. Several techniques to avoid these problems have been proposed such as additional measurements and error analysis techniques [83, 84, 85, 86, 87, 88, 89, 90].

The main multi-wavelength methods for determination of optical constants of thin films are based on the Kramers-Kronig relation or on curve fitting with the aid of dispersion equations. The values of n and k obtained in this way are interdependent, and this limits the number of solutions. The fact that transmittance, reflectance or both are measured over an extended spectral region also reduces the likelihood of multiple solutions. Some multi-wavelength methods are also relatively insensitive to random measurement errors.

The Kramers-Kronig methods [91, 92, 93] require that the reflectance or transmittance of the substrate-film combination be known for all wavelengths. However, in practice measurements are not available for all wavelengths, and so corrections have to be applied. These can introduce uncertainties in $n(\lambda)$ and $k(\lambda)$ in the neighborhood of the two ends of the wavelength spectrum used in the measurements. In the multi-wavelength curve fitting methods [51, 94, 95] the dispersion of the optical constants is represented by dispersion equations. These can be based on theoretical considerations or on analytical formulas. In the former case causality conditions are satisfied. The initial estimates of the constants of these equations are then gradually adjusted until a fit between the experimental measurements and the values calculated from the thin film formula is obtained. The advantage of this approach is that the measurements and the fit need not extend beyond the spectral range of interest. However, the assumption that the dispersion of the optical constants can be adequately represented by such simple models is not always justified.

Ellipsometry consists of the measurement of the change in polarization state of a beam of light upon reflection from or transmission through the sample of interest. It is one of the most popular among the methods due to its relative simplicity and capability of characterizing very thin layers. There is also a great number of different hardware configurations which have been used to perform experiments and have proven commercially successful for research and production applications [96]. However to avoid problems of single-wavelength measurements, the recent development of spectroscopic ellipsometry has provided a powerful tool to characterize both single and multilayer stacks [97, 98, 99]. The experimental data are fitted by adjusting the coefficients of the

dispersion equations describing $n(\lambda)$ and $k(\lambda)$ and the thickness of the layer. The critical step involved in the fitting is a proper selection of the dispersion equations.

Dobrowolski *et al.* introduced a multi-wavelength characterization method, known as inverse synthesis [51], where a thin film synthesis program is used to derive the optical parameters from the measured spectral transmittance or reflectance data. The program adjusts the dispersion parameters until good fit between calculated and measured spectral curves is found. The optical constants do not necessarily have to have physical meaning since the equations are only used to describe the convenient $n(\lambda)$ and $k(\lambda)$ parameters that are required to fit the measurement data. However, this is not a problem, as it is not always obvious that optical parameters in bulk materials and thin film structures would be the same. The main criteria when selecting adequate dispersion equations is their capability of describing $n(\lambda)$ and $k(\lambda)$ parameters with the least possible number of constants in the dispersion formulas.

For measured spectral transmittance or reflectance the adjustment of the optical parameters is carried out by minimizing the merit function M representing discrepancy between model and measurements [51].

$$M = \sqrt{\frac{1}{m}\sum_{i=1}^{m}\left(\frac{C_i - E_i}{\varepsilon_i}\right)^2} \quad , \tag{4}$$

where merit function M is defined in terms of difference between the calculated C_i and experimentally measured E_i values of any desired combination of m photometric quantities. The measurement accuracy of the ith photometric quantity is taken into account with ε_i. This normalization is important for balanced solution of the data. The merit function depends on the optical parameters of the thin film layer structure. To find the unknown parameters d, $n(\lambda)$ and $k(\lambda)$ of a thin film layer system, initial parameters are refined gradually until the minimum value of the merit function is found.

The method of inverse synthesis has also been adopted in this work [P3]. It has the benefit of using all available spectral data unlike the relatively simple envelope methods [100, 101, 102], where the analysis is based on the mathematical relation of the maxima and minima in the measured transmittance or reflectance spectra. Moreover inverse synthesis allows to increase the sensitivity or to avoid convergence to a spurious solution in the case of demanding coatings such as metal or semiconductor films. For this purpose the merit function can be utilized to cover spectrophotometric measurements at various angles of incidence.

3.3 Characterization of optical thin films in various angles of incidence

In the optical metrology of thin-film coatings, characterization techniques based on least-squares fitting to the measured reflectance or transmittance spectra are widely used [51, 94, 95, P3]. The fitted spectral characteristics usually consist of the normal-incidence transmittance measurement results. However, the analysis may also include spectrophotometric measurement data collected at oblique angles of incidence. Moreover,

the reflectance measurements are almost always made at oblique incidence. Thus in order to compare the reflectance and the transmittance measurement results, the transmittance data at the oblique incidence may also be needed. Furthermore, the oblique-incidence data can increase the sensitivity of the characterization methods [51, P3].

It is obvious that the accuracy of the characterization procedures based on curve fitting to the spectrophotometric data is highly related to the quality of the measurements. The uncertainty in the determined optical parameters of a thin-film layer is a result of various uncertainty components in the measurements, especially of those having systematic origin [103, 104]. Furthermore, there are additional systematic factors that require careful consideration when the spectrophotometric measurements are performed at oblique angles of incidence, such as misalignment between the polarization and the incidence planes, angle determination error, and quality of the beam collimation [105]. At the TKK, it is possible to carry out spectrophotometric measurements that satisfy such high requirements [50, 37, 106].

The spectral transmittance and reflectance of a SiO_2 thin-film sample have been measured over the visible to near infrared wavelength regions, 400 – 1600 nm, with collimated linearly-polarized beams incident on the sample at incidence angles ranging from normal incidence to the Brewster's angle. The results for spectral reflectance and transmittance are presented in Figure 15 and Figure 16, respectively. The optical parameters of the layer determined from each of the oblique incidence reflectance spectra were compared to those derived from the transmittance measurements [P3].

The intercomparison shows a good agreement among the optical parameters derived from the reflectance data at the different angles of incidence and among those from the normal and oblique-incidence transmittance characterization. The agreement among the results is within 0.2 % [P3]. Thus the good agreement among the determined optical parameters supports the accuracy of the measurements with the two instruments and consistency in determining the incidence angles, alignment of the plane of polarization with respect to the plane of incidence, and also a good collimation of the measurement beams. These factors have to be considered carefully in the oblique-incidence spectrophotometric measurements, especially when ordinary commercial spectrophotometers with converging beam geometries are used. Otherwise they could cause significant systematic errors in the determined optical parameters of the layer. For the first time, this confirms the reliability and accuracy of the used technique in the characterization of thin films [P3].

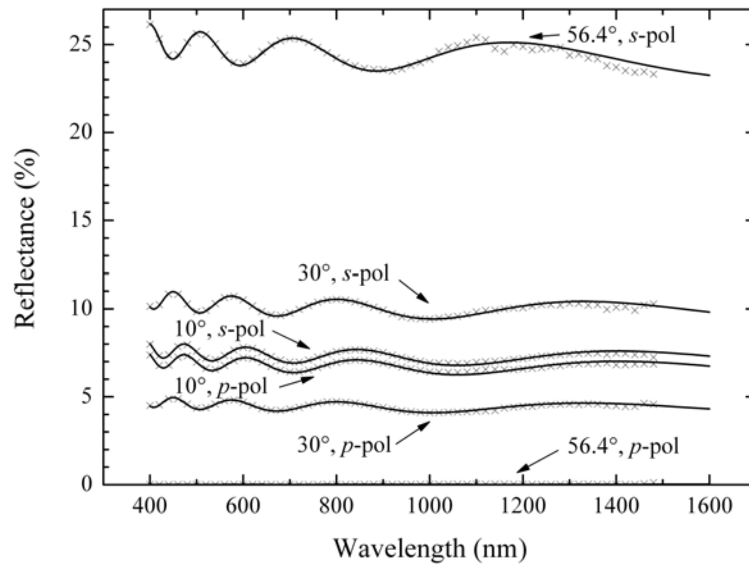

Figure 15. Reflectance of the 720 nm thick SiO_2 thin film layer deposited on a fused quartz substrate. Crosses represent measured values and solid lines modeled values. [P3]

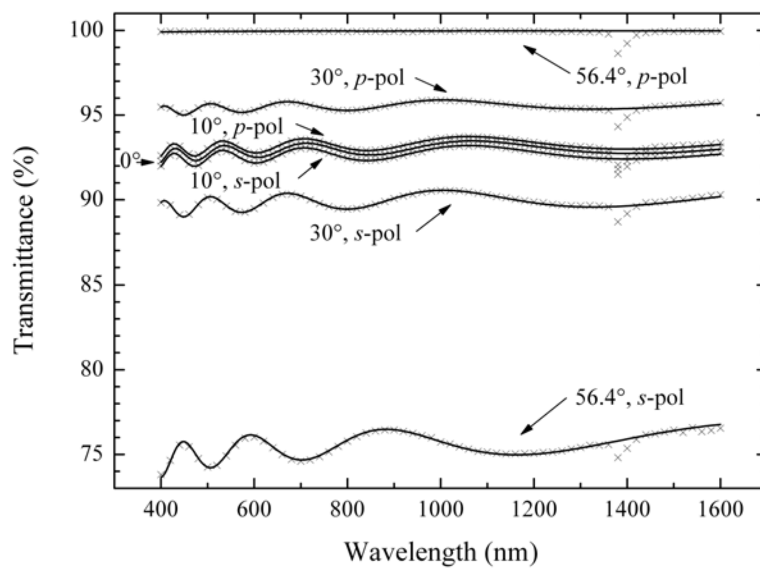

Figure 16. Transmittance of the 720 nm thick SiO_2 thin film layer deposited on a fused quartz substrate. Crosses represent measured values and solid lines modeled values. [P3]

4 Measurement of optical fiber nonlinearity

4.1 Nonlinear refractive index

Nonlinear interactions between light and silica fiber start to arise, when high powers are used. The response of any dielectric material to light becomes nonlinear for intense electromagnetic fields and several nonlinear effects influence to propagation of light. The severity of these nonlinear effects in optical fibers can also be affected by different dopants in the fiber core and cladding, such as GeO_2 and Al_2O_3. The total polarization **P** is not linear with respect to the electric field **E** but it can be written as [26]

$$\mathbf{P} = \varepsilon_0 \left(\chi^{(1)} \cdot \mathbf{E} + \chi^{(2)} \cdot \mathbf{E} \cdot \mathbf{E} + \chi^{(3)} \cdot \mathbf{E} \cdot \mathbf{E} \cdot \mathbf{E} + \cdots \right), \quad (5)$$

where ε_0 is the vacuum permittivity and $\chi^{(j)}$ (j = 1,2,…) is j^{th} order susceptibility. The linear susceptibility $\chi^{(1)}$ represents the dominant contribution to **P**. It is included in the refractive index n and the attenuation constant α. The second order susceptibility $\chi^{(2)}$ is responsible for nonlinear effects such as second-harmonic generation and sum-frequency generation. However, these phenomena arise from the lack of inversion symmetry of the material. As SiO_2 is a symmetrical molecule, the second-order susceptibility normally vanishes.

The lowest-order nonlinear effects in the optical fibers originate from the third-order susceptibility $\chi^{(3)}$, which is responsible for such phenomena as third-harmonic generation, four-wave mixing (FWM) and nonlinear refraction. Most of the nonlinear effects in optical fiber arise from the nonlinear refraction, a phenomenon referring to the intensity dependence of the refractive index. The relation between the refractive index n, intensity I and power P is

$$n = n_0 + n_2 I = n_0 + \left(\frac{n_2}{A_{\text{eff}}} \right) P \ , \quad (6)$$

where the first term n_0 is the wavelength-dependent part of the refractive index and A_{eff} is the effective area of the optical fiber. The second term, nonlinear refractive index, n_2, collects up intensity-dependent nonlinear effects. The most interesting effects of this group are self-phase modulation (SPM), cross-phase modulation (XPM) and FWM. Because all of the above-mentioned effects are intensity-dependent and optical fiber has relatively low value of nonlinear susceptibility $\chi^{(3)}$, these effects are visible only at high powers.

The nonlinear coefficient is defined as n_2/A_{eff} [107]. Therefore, it can be measured without knowing the effective area of the optical fiber. However, the impact of the nonlinear effects depends also on the axial distribution of power inside the optical fiber. If the effective area is increased, then the influence of the intensity dependent nonlinear effects is reduced.

In the literature, the nonlinearity of optical fibers is often expressed with so called nonlinear parameter γ, which is related to the nonlinear refractive index n_2 as

$$\gamma = \frac{\omega_0 n_2}{c_0 A_{\text{eff}}} = \frac{2\pi}{\lambda_0} \frac{n_2}{A_{\text{eff}}} \ , \tag{7}$$

where ω_0 represents the angular frequency of the light wave, c_0 is the speed of light in vacuum, λ_0 is the wavelength in vacuum and A_{eff} is the effective area of the optical fiber. In general, n_2 is related to χ for linear polarization as [26]

$$n_2 = \frac{3}{8n} \chi^{(3)}_{xxxx} \ . \tag{8}$$

Where $\chi^{(3)}$ is the third-order susceptibility and x represents one direction of the principal axes. The optical field is assumed to be linearly polarized, and therefore only one component of the fourth-rank tensor contributes to the refractive index.

4.2 Nonlinear light propagation in optical fibers

Pulse propagation in fibers can be described by Nonlinear Schrödinger Equation (NLSE) [26]:

$$\frac{\partial A}{\partial z} + \beta_1 \frac{\partial A}{\partial t} + \frac{i\beta_2}{2} \frac{\partial^2 A}{\partial t^2} + \frac{\alpha}{2} A = i\gamma |A|^2 A \ , \tag{9}$$

where A is the pulse amplitude that is assumed to be normalized such that $|A|^2$ represents the optical power. NLSE equation includes the effects of fiber losses through α, chromatic dispersion through β_1 and β_2, and fiber nonlinearity through γ.

The dispersion parameter D is related to propagation constants β_1 and β_2 by the relation [26]:

$$D = \frac{d\beta_1}{d\lambda} = -\frac{2\pi c}{\lambda^2} \beta_2 \approx \frac{\lambda}{c_0} \frac{d^2 n}{d\lambda^2} \ , \tag{10}$$

where c_0 is the speed of light in vacuum, λ is the wavelength in vacuum, and n is the refractive index.

Pulses at different wavelengths propagate at different speeds inside a fiber because of a mismatch in their group velocities. However, the group velocity dispersion can be neglected for relatively long pulses ($T_0 > 100$ ps) with a large peak power ($P_0 > 1$ W) [26]. As a result, the term β_2 can be set to zero in Equation 9. Now, the SPM gives rise to an intensity-dependent nonlinear phase shift φ_{SPM} presented in Equation 18. In order to derive this, normalized amplitude, U, is defined by [26]

$$A(z,T) = \sqrt{P_0} e^{-\alpha z/2} U(z,\tau) \ , \tag{11}$$

where A is the slowly varying amplitude of the pulse, P_0 is the peak power of the incident pulse, α represents losses, and τ is the normalized time scale proportional to the input pulse width T_0. The τ is defined as

$$\tau = \frac{T}{T_0} = \frac{t - z/v_g}{T_0} \quad , \tag{12}$$

where v_g is the group velocity, and T is measured pulse width in a frame of reference moving with the pulse at group velocity after pulse has propagated time t and distance z in the fiber.

Now, the pulse-propagation equation [26] can be written with normalized amplitude as

$$\frac{\partial U}{\partial z} = \frac{ie^{-\alpha z}}{L_{\mathrm{NL}}} |U|^2 U \quad , \tag{13}$$

where α accounts for fiber losses. The nonlinear length L_{NL} is defined as [26]

$$L_{\mathrm{NL}} = \frac{1}{\gamma P_0} \quad , \tag{14}$$

where P_0 is the peak power and γ is related to nonlinear refractive index as in Equation 7. Equation 13 can be solved directly to obtain the general solution

$$U(L,T) = U(0,T) e^{i\varphi_{\mathrm{NL}}(L,T)} \quad , \tag{15}$$

Where $U(0,T)$ is the field amplitude at $z = 0$ and nonlinear phase shift is

$$\varphi_{\mathrm{NL}}(L,T) = |U(0,T)|^2 \left(\frac{L_{\mathrm{eff}}}{L_{\mathrm{NL}}} \right) \tag{16}$$

with the effective length L_{eff} defined as [108]

$$L_{\mathrm{eff}} = \frac{1}{P_0} \int_0^L P_0 e^{-\alpha z} dz = \frac{1 - e^{-\alpha L}}{\alpha} \quad , \tag{17}$$

where P_0 is the optical power launched into the fiber and α is the attenuation constant. This simple model assumes that the power is constant over a certain effective length L_{eff}. It has proven to be quite sufficient in estimating the effect of nonlinearities, as most of the nonlinear effects occur in the beginning of the fiber.

Equation 15 shows that SPM gives rise to the intensity-dependent phase shift but the pulse shape remains unaffected. The nonlinear phase shift φ_{NL} increases with fiber length. In the absence of fiber losses $\alpha = 0$ and $L_{\mathrm{eff}} = L$, the maximum phase shift φ_{SPM} occurs at

the pulse center located at $T = 0$. With U normalized such that $|U(0,0)| = 1$, it is given by

$$\varphi_{\mathrm{SPM}} = \frac{L_{\mathrm{eff}}}{L_{\mathrm{NL}}} = \gamma P_0 L_{\mathrm{eff}} \ . \tag{18}$$

4.3 Continuous-wave self-phase modulation method

The method of continuous-wave self-phase modulation (CW SPM) for the measurement of nonlinear coefficient of optical fibers was first introduced by Boskovic *et al.* in 1996 [109]. Since then the method has been widely adopted by optical fiber measurement community [110, 111, 112]. However, the name of the technique is inconsistent in the literature. The same measurement principle is sometimes referred as four-wave mixing (FWM) method, as e.g. in [110], due to the fact that generated sidebands can also be interpreted as FWM product. Even though this could be a more descriptive name, there are several reasons to use the term CW SPM instead of FWM. When the CW SPM method was first introduced [109] the authors explained the generation of optical sidebands using nonlinear phase shift. Due to this mathematical description, probably similar to the one presented in Chapter 4.2, the method has traditionally been considered as SPM method. Nowadays, it is also an established convention to separate this well-known method from other techniques, referred as FWM methods [113, 114, 115, 116, 117], utilizing measurement of optical sidebands.

In addition to these methods to determine the nonlinear coefficient of optical fibers, also techniques utilizing pulsed light source and self-phase modulation (P-SPM) [76, 118, 119], cross-phase modulation (XPM) [120, 121] and modulation instability [122] have remained in use. No method has been clearly superior compared to others [123] and so far no standard methods have been proposed by International Telecommunication Union (ITU). However, the standardization work is in process [107] and the CW SPM method is one of the strongest candidates to be among the standardized methods.

The strength of the CW SPM method lies in the straightforward measurement scheme and fairly good repeatability [110], when compared to other techniques. At TKK, we utilized the CW SPM method as outlined in Figure 17 [P5]. Two continuous-wave external cavity diode lasers (ECDL) were operated at around 1550 nm. The output beams were set to have the same linear polarization using polarization controllers and a polarizer after the beams were combined. The beat signal was then amplified and launched into the fiber under test (FUT). The length of the fiber samples, L, varied from 100 m to 3000 m. The optical power was measured at the end of the tested fiber. The total attenuation of the 99 % branch of the coupler and the tested fiber were taken into account by carefully characterizing their attenuation.

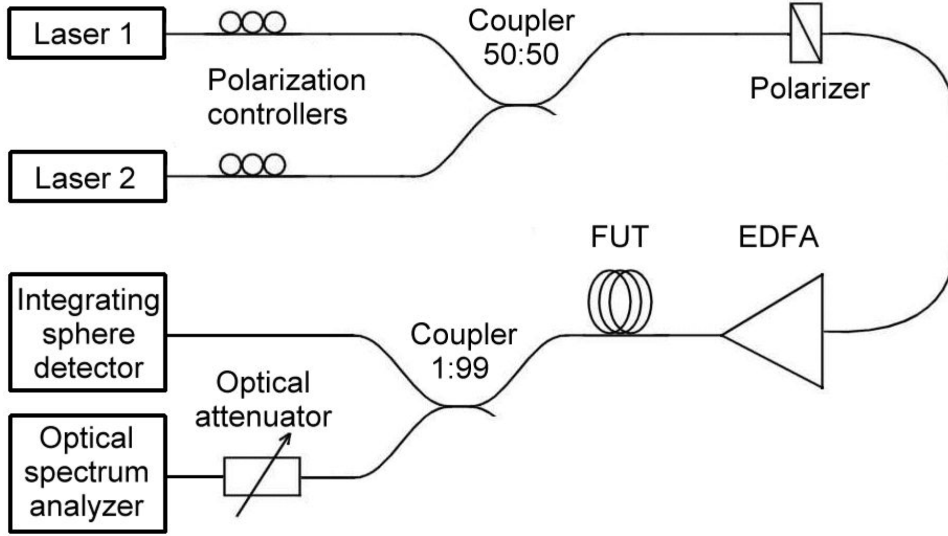

Figure 17. Measurement setup of continuous-wave self-phase modulation method. [P5]

In CW SPM-method only peak heights of the fundamental waves and first-order sidebands are measured from the spectrum. Starting from Equation 16, where nonlinear phase-shift induced by SPM is presented, we can derive the relationship between the measured intensity peaks I_0, I_1 and nonlinear phase-shift φ_{SPM}. The FUT has two different input signals with same amplitude, $E_1 = E_2$, but different frequencies ω_1 and ω_2:

$$U(0,T) = E_1 \sin(\omega_1 T) + E_2 \sin(\omega_2 T) \ . \tag{19}$$

This signal can be substituted into Equation 16 to get the nonlinear phase-shift

$$\varphi_{NL}(L,T) = \left|E_1 \sin(\omega_1 T) + E_2 \sin(\omega_2 T)\right|^2 \left(\frac{L_{eff}}{L_{NL}}\right) . \tag{20}$$

Now, it is possible to solve the normalized field amplitudes after the light has propagated distance L in the fiber. Equation 20 can be substituted into Equation 15 to get the following form

$$\begin{aligned} U(L,T) &= [E_1 \sin(\omega_1 T) + E_2 \sin(\omega_2 T)] e^{i\left|E_1 \sin(\omega_1 T) + E_2 \sin(\omega_2 T)\right|^2 \left(\frac{L_{eff}}{L_{NL}}\right)} \\ &= [E_1 \sin(\omega_1 T) + E_2 \sin(\omega_2 T)] e^{i\left[E_1^2 \sin^2(\omega_1 T) + 2E_1 E_2 \sin(\omega_1 T)\sin(\omega_2 T) + E_2^2 \sin^2(\omega_2 T)\right]\left(\frac{L_{eff}}{L_{NL}}\right)} \\ &= [E_1 \sin(\omega_1 T) + E_2 \sin(\omega_2 T)] e^{i\left[\frac{E_1^2}{2}(1-\cos(2\omega_1 T)) + E_1 E_2 (\cos[(\omega_1-\omega_2)T] - \cos[(\omega_1+\omega_2)T]) + \frac{E_1^2}{2}(1-\cos(2\omega_1 T))\right]\left(\frac{L_{eff}}{L_{NL}}\right)} \\ &= [E_1 \sin(\omega_1 T) + E_2 \sin(\omega_2 T)] e^{i\left[(E_1^2 + E_1^2) - E_1^2 \cos(2\omega_1 T) + 2E_1 E_2 \cos[(\omega_1-\omega_2)T] - 2E_1 E_2 \cos[(\omega_1+\omega_2)T] - E_2^2 \cos(2\omega_1 T)\right]\left(\frac{\varphi_{SPM}}{2}\right)} \end{aligned} \ . \tag{21}$$

It is possible to generate Bessel functions from the exponents of the above equation, by using the following Bessel function expansion [124]

$$e^{ix\cos(\varphi)} = \sum_{n=-\infty}^{\infty} i^n J_n(x) e^{in\varphi} \ , \tag{22}$$

where J_n is the Bessel function of the nth order. All the terms have an imaginary factor i^n, which will be cancelled out later from the significant terms, when the terms of the infinite Bessel function series are multiplied with each other.

$$\begin{aligned} U(L,T) = {} & [E_1 \sin(\omega_1 T) + E_2 \sin(\omega_2 T)] e^{i\left[E_1^2 + E_1^2\right]\left(\frac{\varphi_{\text{SPM}}}{2}\right)} \\ & \times \left(\sum_{n=-\infty}^{\infty} i^n J_n\left(\frac{\varphi_{\text{SPM}}}{2}\right) e^{in(2\omega_1)T} \right) \left(\sum_{n=-\infty}^{\infty} i^n J_n\left(\frac{\varphi_{\text{SPM}}}{2}\right) e^{in(\omega_1 - \omega_2)T} \right) \\ & \times \left(\sum_{n=-\infty}^{\infty} i^n J_n\left(\frac{\varphi_{\text{SPM}}}{2}\right) e^{in(\omega_1 - \omega_2)T} \right) \left(\sum_{n=-\infty}^{\infty} i^n J_n\left(\frac{\varphi_{\text{SPM}}}{2}\right) e^{in(\omega_1 + \omega_2)T} \right) \\ & \times \left(\sum_{n=-\infty}^{\infty} i^n J_n\left(\frac{\varphi_{\text{SPM}}}{2}\right) e^{in(\omega_1 + \omega_2)T} \right) \left(\sum_{n=-\infty}^{\infty} i^n J_n\left(\frac{\varphi_{\text{SPM}}}{2}\right) e^{in(2\omega_2)T} \right) \end{aligned} \tag{23}$$

Using the Euler formula [124],

$$\sin(\theta) = \frac{e^{i\theta} + e^{-i\theta}}{2i} \ , \tag{24}$$

to the to sine-terms of the Equation 23. We will obtain an equation

$$\begin{aligned} U(L,T) = {} & \frac{1}{2i} \left[E_2 \left(e^{i\omega_1 T} - e^{-i\omega_1 T} \right) + E_2 \left(e^{i\omega_2 T} - e^{-i\omega_2 T} \right) \right] e^{i\left[E_1^2 + E_1^2\right]\left(\frac{\varphi_{\text{SPM}}}{2}\right)} \\ & \times \left(-\sum_{n=-\infty}^{\infty} i^n J_n\left(\frac{\varphi_{\text{SPM}}}{2}\right) e^{in(2\omega_1)T} \right) \left(\sum_{n=-\infty}^{\infty} i^n J_n\left(\frac{\varphi_{\text{SPM}}}{2}\right) e^{in(\omega_1 - \omega_2)T} \right) \\ & \times \left(\sum_{n=-\infty}^{\infty} i^n J_n\left(\frac{\varphi_{\text{SPM}}}{2}\right) e^{in(\omega_1 - \omega_2)T} \right) \left(-\sum_{n=-\infty}^{\infty} i^n J_n\left(\frac{\varphi_{\text{SPM}}}{2}\right) e^{in(\omega_1 + \omega_2)T} \right) \\ & \times \left(-\sum_{n=-\infty}^{\infty} i^n J_n\left(\frac{\varphi_{\text{SPM}}}{2}\right) e^{in(\omega_1 + \omega_2)T} \right) \left(-\sum_{n=-\infty}^{\infty} i^n J_n\left(\frac{\varphi_{\text{SPM}}}{2}\right) e^{in(2\omega_2)T} \right) \end{aligned} \tag{25}$$

These infinite series of Bessel functions contain exponent terms, which are modulating the phase of the input waveform. Therefore, it leads to the generation of 1st, 2nd, 3rd, etc. sidebands. The generation of new frequencies is presented in Figure 18. Only the terms that contribute to the intensities of the fundamental or 1st order sidebands are taken into account, because even the power transferred to the 1st order sidebands is orders of

magnitude lower than the power in the input frequencies. Respectively, the power of the 2nd order sidebands is considerably smaller than the power of the 1st order sidebands.

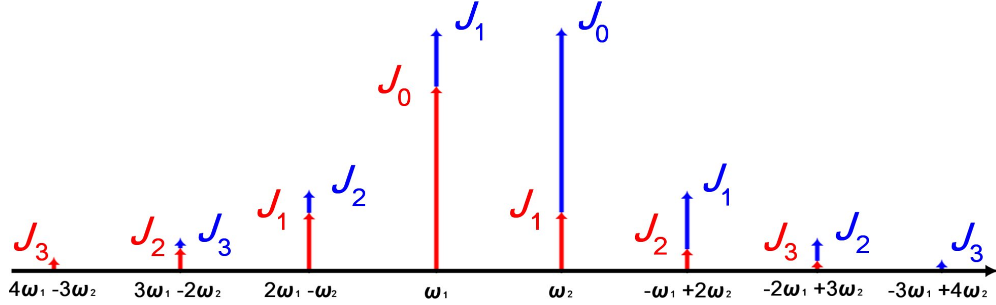

Figure 18. Dual-frequency signal (ω_1 and ω_2) will generate new frequencies due to SPM. These frequencies are determined by the frequency of the beat signal (ω_2 - ω_1).

This modulation will generate following intensities to the fundamental wavelengths (0th order) and 1st order sidebands:

$$
\begin{array}{l}
0^{\text{th}}\text{ order}\left\{\begin{array}{r}
J_0^6\left(\frac{\varphi_{\text{SPM}}}{2}\right)\left[\left(e^{i\omega_1 T}-e^{i\omega_1 T}\right)+\left(e^{i\omega_2 T}-e^{i\omega_2 T}\right)\right]C \\
J_0^4\left(\frac{\varphi_{\text{SPM}}}{2}\right)J_1^2\left(\frac{\varphi_{\text{SPM}}}{2}\right)\left[\left(e^{i\omega_1 T}-e^{i\omega_1 T}\right)+\left(e^{i\omega_2 T}-e^{i\omega_2 T}\right)\right]C
\end{array}\right. \\
1^{\text{st}}\text{ order}\left\{\begin{array}{l}
J_0^4\left(\frac{\varphi_{\text{SPM}}}{2}\right)J_1^2\left(\frac{\varphi_{\text{SPM}}}{2}\right)\left[\left(e^{i(2\omega_1-\omega_2)T}-e^{i(2\omega_1-\omega_2)T}\right)+\left(e^{i(-\omega_1+2\omega_2)T}-e^{i(-\omega_1+2\omega_2)T}\right)\right]C \\
J_0^4\left(\frac{\varphi_{\text{SPM}}}{2}\right)J_2^2\left(\frac{\varphi_{\text{SPM}}}{2}\right)\left[\left(e^{i(2\omega_1-\omega_2)T}-e^{i(2\omega_1-\omega_2)T}\right)+\left(e^{i(-\omega_1+2\omega_2)T}-e^{i(-\omega_1+2\omega_2)T}\right)\right]C
\end{array}\right.
\end{array}, \quad (26)
$$

where C is a constant, containing products of the amplitudes E_1 and E_2, and ½i-term from the sine-function of the Euler formula.

When high optical power is coupled into the fiber, sidebands lying symmetrically around the fundamental wavelengths are generated due to self-phase modulation [109]. In Figure 19, optical spectrum containing fundamental wavelengths at intensity I_0 and first side bands at intensity I_1 is shown. Second sidebands lie about two orders of magnitude below the first sidebands and the power transferred to the higher order sidebands can be neglected. Therefore, only Bessel functions of second order or lower can take part to the generation of the frequencies of the intensity of the input waveform I_0 and the intensity of the 1st sidebands I_1. When 0th order terms are divided by 1st order terms from Equation 26, we will get the intensity ratio I_0/I_1 of the fundamental wavelengths to the first sidebands, the nonlinear phase shift φ_{SPM} of the signal can be obtained from

$$\frac{I_0}{I_1}=\frac{J_0^6\left(\varphi_{\mathrm{SPM}}/2\right)+J_0^4\left(\varphi_{\mathrm{SPM}}/2\right)J_1^2\left(\varphi_{\mathrm{SPM}}/2\right)}{J_0^4\left(\varphi_{\mathrm{SPM}}/2\right)J_1^2\left(\varphi_{\mathrm{SPM}}/2\right)+J_0^4\left(\varphi_{\mathrm{SPM}}/2\right)J_2^2\left(\varphi_{\mathrm{SPM}}/2\right)}=\frac{J_0^2\left(\varphi_{\mathrm{SPM}}/2\right)+J_1^2\left(\varphi_{\mathrm{SPM}}/2\right)}{J_1^2\left(\varphi_{\mathrm{SPM}}/2\right)+J_2^2\left(\varphi_{\mathrm{SPM}}/2\right)}\ , \quad (27)$$

where J_n are Bessel functions of the nth order [109]. The nonlinear coefficient n_2/A_{eff} can then be found from the relation [109],

$$\frac{n_2}{A_{\mathrm{eff}}}=\frac{\lambda_0}{4\pi L_{\mathrm{eff}}}\left(\frac{\varphi_{\mathrm{SPM}}}{P_{\mathrm{AVG}}}\right)=\frac{\lambda_0}{4\pi L_{\mathrm{eff}}}k_{\mathrm{ac}}\ , \quad (28)$$

by plotting the nonlinear phase shift φ_{SPM} as a function of the average power of the signal, P_{AVG}. In Equation 28, λ_0 is the center wavelength in vacuum, and L_{eff} and A_{eff} are the effective length [108] and the effective area [26] of the fiber, respectively. A value for the nonlinear coefficient is obtained from the slope of the line, k_{ac}, fitted to the measurement data [P4]. Figure 20 shows the measurement data for several SMF lengths together with the fitted lines. The above analysis neglects the effects of fiber dispersion.

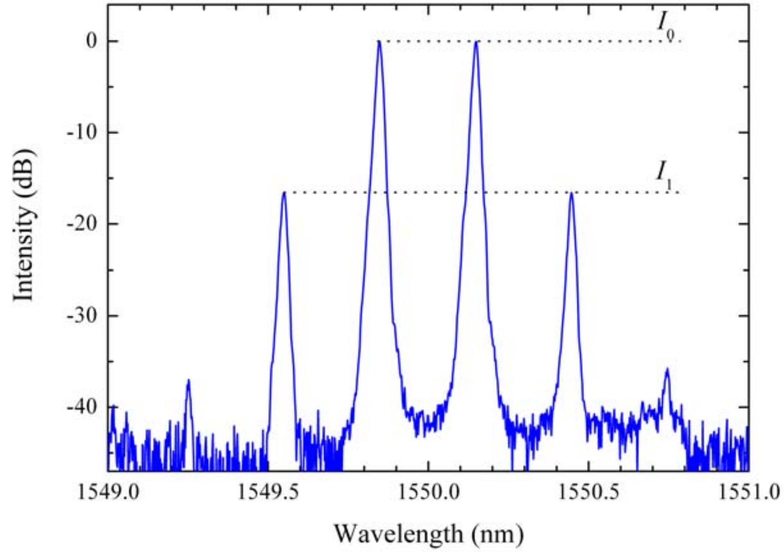

Figure 19. Optical spectrum measured from 500 m single-mode fiber (SMF) using 27.6 dBm input power in dual-frequency signal. Fundamental wavelengths are separated 0.3 nm from each other. Symmetric sidebands of first and second order are generated.

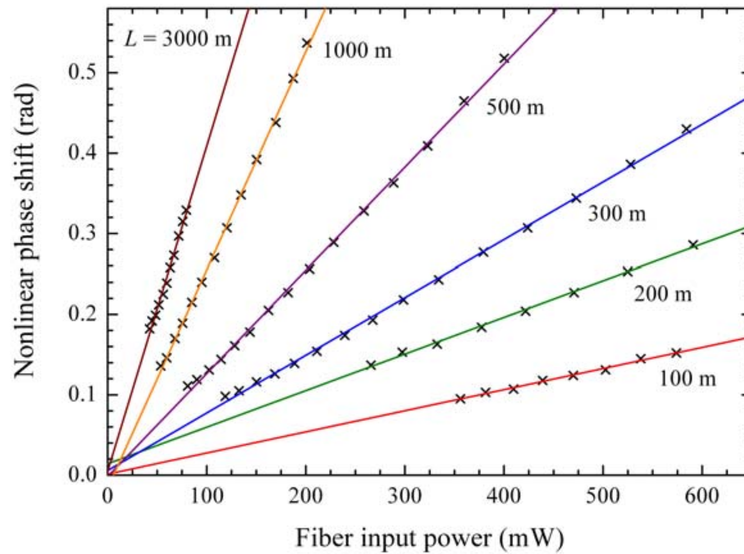

Figure 20. Nonlinear phase shifts for SMF of various lengths. The measurement power range is limited by noise level and stimulated Brillouin scattering at low and high power level sides, respectively. [P4]

4.4 Effects of dispersion

In telecommunication applications fiber dispersion and chirp can set limitations to optical system performance. Same phenomena can cause systematic errors for the determination of fiber nonlinearity, when the wavelengths of interest experience effects of fiber dispersion. As the light propagates inside a dispersive medium, the phase matching conditions between two fundamental wavelengths will vary resulting, in most of the cases, lowered apparent value for nonlinear coefficient. The severity of the dispersion effects depends greatly on the measurement conditions [P4, P5, 111, 112], but in the early studies of nonlinear refractive index, the effects of dispersion were either neglected or the measurement conditions were adjusted to avoid the significant influence of the fiber dispersion [109]. However, fiber dispersion can cause systematic shift of several percent in the value of nonlinear coefficient even with SMFs having a moderate dispersion parameter D = 16 ps/nm·km [P4, P5, 111, 112].

K. Nakajima *et al.* have been determining the measurement conditions for measuring the nonlinear refractive index of optical fibers, where the effects of fiber dispersion would be minimal [111]. This approach limits the measurement conditions to the individual cases, which vary depending on the fiber length, dispersion, wavelength separation of the fundamental waves and used optical power. By combining measurements with simulations using NLSE [26, 125], it is possible to develop a more generic approach for different measurement conditions [P4]. If the measurement results in Figure 21 are evaluated without taking dispersion into account, the value of nonlinear coefficient is underestimated by ~ 2 % due to the result of imperfect fitting to the measurement data.

By taking the dispersion into account in the fitting using NLSE, the phase shift curves are not straight lines anymore, but tend to bend slightly upwards in the case of anomalous dispersion. This will result in a significantly better fit, as the quality of the fitting is evaluated with the least-squares method [P5].

Even though the dispersion affects the determination of n_2/A_{eff} typically a few percent with standard single-mode fibers (SMFs), the effects of dispersion can be drastic with special fibers [P4]. In Figure 22a, the phase shift curves simulated for SMF having anomalous dispersion of 16 ps/nm·km are only slightly bending upwards. Similar behavior takes place with non-zero dispersion shifted fiber (NZ-DSF) having anomalous dispersion of 6.8 ps/nm·km. In the case of dispersion compensating fiber (DCF) having normal dispersion of 110 ps/nm·km, the phase shift curves bend downwards. The bending of phase shift curves, results in variations in apparent values of n_2/A_{eff}, as shown in Figure 22b, if the dispersion is not taken into account. The apparent results can therefore become significantly erroneous.

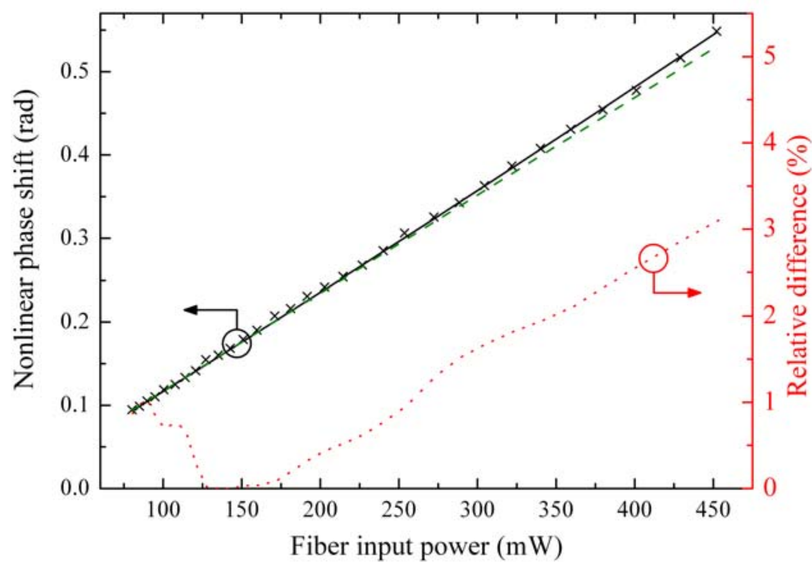

Figure 21. Relative difference (dotted red line) between nonlinear phase shifts determined either by using traditional model (dashed green line) or model that takes dispersion into account (solid black line). Crosses present measured values. [P5]

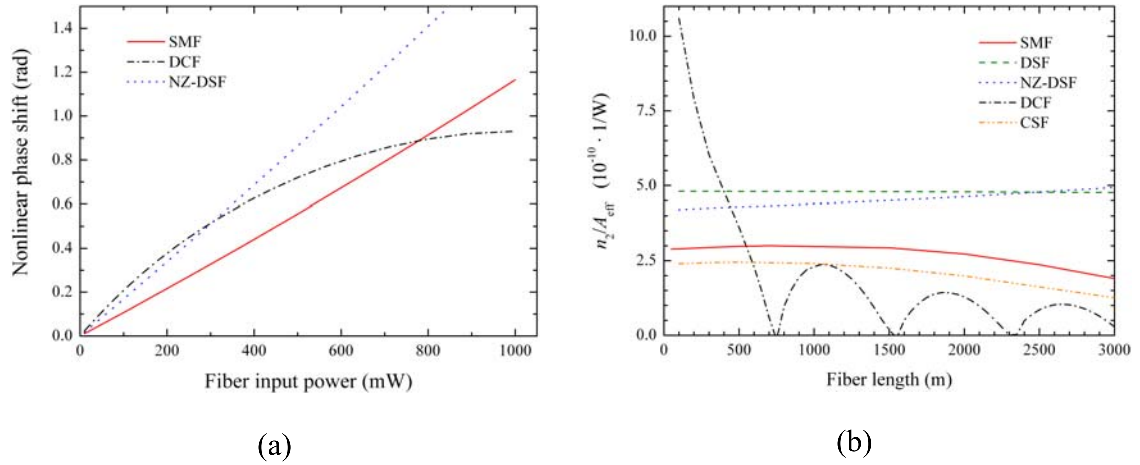

Figure 22. Simulated (a) Nonlinear phase shift curves and (b) apparent values for nonlinear coefficient for various single mode fibers.

The nonlinear refractive index and nonlinear coefficient are physical parameters related to optical fibers. Therefore their values should be independent on measurement conditions. Another example demonstrating the dispersion effects on the determination of the nonlinear coefficient is presented in Figure 23, where the wavelength separation between the fundamental waves used in CW SPM method is varied. The measurements are in good agreement with simulations utilizing NLSE. With the approach completely neglecting fiber dispersion, it is impossible to take into account that apparent results of the nonlinear coefficient will vary as a function of wavelength separation. Unfortunately, this condition of fixed nonlinear coefficient is true only in a special case, where the dispersion parameter is set to $D = 0$. When NLSE simulations are used, the value of n_2/A_{eff} giving the best fit to the measurement data can be interpreted as a physical value. As mentioned earlier, the value of the nonlinear coefficient acquired with this method is independent of the measurement conditions.

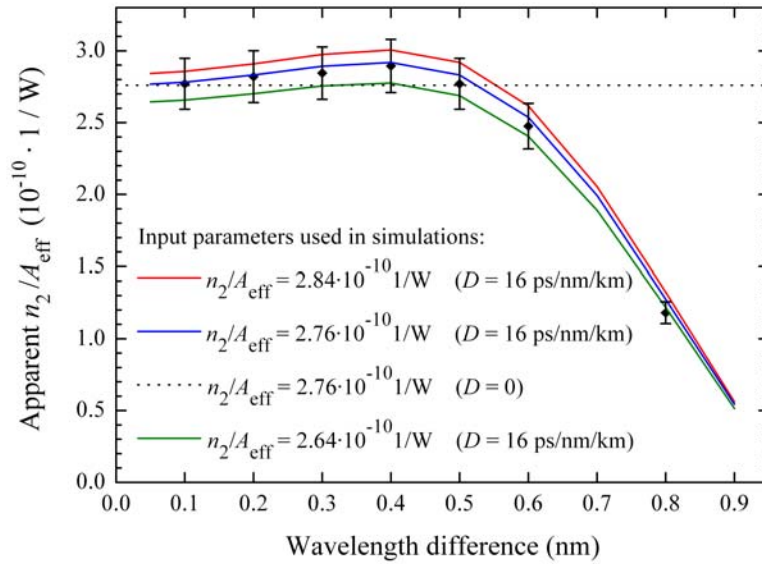

Figure 23. Fiber dispersion affects the apparent values on n_2/A_{eff}. Measurements are performed for 500 m long SMF with power range of 19 to 26 dBm. [P4]

4.5 Measurement of high fiber optic power

If uncalibrated instruments are used, significant systematic errors can occur in determination of fiber nonlinearity as the nonlinear phase shift is directly proportional to the value of optical power as presented in Equation 6. At TKK, we use the integrating sphere (ISP) detector which is designed for high fiber optic power. The detector is described in more detail in Chapter 2.5. The traceability chain sets the limits for minimum uncertainty of the ISP detector. The fiber optic power can be measured directly from the output end of the fiber with expanded uncertainty ($k = 2$), corresponding to 95 % level of confidence, of 0.93 % up to 100 mW [72, 77] and of 1.3 % up to 650 mW. The uncertainty component due to determination of the attenuation of the splice and coupler, between the optical power meter and front end of the fiber under test, is 0.7 %. This results in the total power measurement an uncertainty component of 1.5 %.

The difficulty in fiber optic power measurements is often not only the determination of optical power, but the determination of the optical power inside the closed fiber system. We are not interested in the power that couples out of the fiber, but the power launched into the fiber. This can be measured by either using an optical coupler with a known coupling ratio in front of the studied fiber or the power measurements can be performed from the rear end of the measurement setup, as presented in Figure 24. This figure is a close-up from the end part of the measurement setup between EDFA and ISP detector, illustrated in Figure 17. The reason for selecting the rear end measurement scheme is that both alternatives would require characterization of optical attenuations in order to determine the optical power launched into the fiber under test. In addition to this, the use

of the coupler to divide the launched signal in two beam paths would result in a loss of maximum available power for the front end measurement.

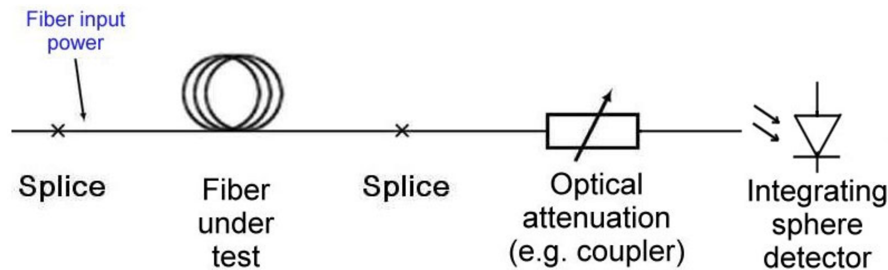

Figure 24. Measurement of fiber optic power in CW SPM method.

4.6 Uncertainty analysis

The development of the measurement techniques for nonlinearity of optical fibers has reached a level, where increased interest should be directed towards improved agreement of the current techniques. It is clearly evident that without better justified uncertainty analyses and concern for the high precision measurements, the results of the intercomparisons between different laboratories will not show their full potential as a tool to improve measurement accuracy.

Several relatively wide intercomparisons containing different techniques and participating laboratories have been performed since the year 1999 [123, 126, 127, 128, 129, 130, 131]. Among them the most recent ITU-T comparison [123] shows that the agreement between participating laboratories is on the order of ± 10 %. Even the four laboratories, all using the CW SPM method did not succeed in obtaining a remarkably better agreement between each other. The further development of the various techniques has not brought the results of various laboratories any closer to each other, as the agreement levels already achieved in earlier comparisons have not improved significantly. The common problem for these comparisons is that the measurement uncertainties of the participating laboratories are not evaluated. Another important issue is that several factors, such as fiber dispersion [111, P4], light polarization state [121, 132, 133, 134] or calibration of the instruments [P5] can cause severe systematic errors to the measurements. The pilot and coordinating institute arranging such comparison measurements should demand sufficient uncertainty analysis from the participating laboratories. On the other hand, the analysis technique of the final comparison results should be known in advance by all the participants.

At the TKK, an effort has been made to estimate the uncertainty contributions related to the CW SPM method. The analysis takes into account several parameters that are directly affecting uncertainty in the determination of n_2/A_{eff}. The measurement of high fiber optic power has remained as the major source of uncertainty, even though it has been improved significantly by replacing the commercial power meter and attenuator with the ISP detector [P4, P5]. Formerly the second biggest uncertainty component, dispersion, is now reduced to the uncertainty level of 0.5 % instead of 3.0 % ($k = 2$) [P5]. Its contribution is now also possible to take into account in much wider range of measurement conditions, as the measurements were earlier limited to the range where dispersion effects remained weak enough. The combination of uncertainty budgets [135] presented in [P4] and [P5] is shown in Table 1.

Table 1. Uncertainty analysis for the CW SPM method realized at the TKK.

Uncertainty component	Relative uncertainty (%)	
	old setup [P4]	improved setup [P5]
Fiber length L	0.4	0.4
Determination of optical power P_{AVG}	5.4	1.5
Optical spectrum analyzer $I_0/I_1 \rightarrow \varphi_{\mathrm{SPM}}$	1.3	1.3
Wavelength uncertainty	0.1	0.1
Contribution of fiber dispersion	3.0	0.5
Expanded uncertainty n_2/A_{eff} ($k = 2$)	6.4	2.0

5 Conclusions

Metrology Research Institute is in the process of extending its spectral responsivity and spectral irradiance scales out of the wavelength band, where traditional Si photodiodes are applicable. For this purpose, the Ge photodetectors have been characterized in the wavelength range of 850 - 1650 nm and the GaAsP trap detector for the range 200 - 600 nm. In this thesis, also a high-accuracy measurement technique using spectrophotometric reflectance and transmittance measurements is used to experimentally characterize optical parameters of SiO_2 thin films at oblique angles of incidence. Finally an integrating sphere detector and mathematical modeling of fiber dispersion are used to improve the determination of nonlinear coefficient of optical fibers n_2/A_{eff}.

The use of Si detectors accompanied with GaAsP and Ge detectors provides a possibility of continuous scale realization of spectral responsivity over the wavelength range of 200 to 1650 nm. Both studied detectors are characterized in terms of spectral responsivity and reflectance and attention is paid to their special characteristics. The Ge detectors have several drawbacks when used as transfer standard detectors, such as low shunt resistance and thus reasonably high dark current. They are also sensitive to temperature changes. However, nowadays large area Ge detectors have good spatial uniformities and they offer cost-effective, yet reasonably accurate, alternative for expensive large area InGaAs photodiodes. The GaAsP trap detector has a decrease in internal quantum efficiency when compared to a single photodiode. This is probably a result of increased absorption in a Schottky contact layer, made of gold, on the top of the photodiodes. Nevertheless, the constructed GaAsP trap detector seems to be suitable to be used as working standard in the ultraviolet wavelength region.

The high accuracy spectrophotometric measurements are carried out in order to characterize the SiO_2 thin film layer deposited on a fused quartz substrate. The spectral reflectance and transmittance measurements performed in various incidence angles from normal to Brewster's angle are compared successfully for the first time ever. The consistency of ~ 0.2 % in the results confirms the quality of the spectrophotometric measurements and the characterization method. When measurements are performed at oblique angles of incidence, several systematic factors, such as quality of beam collimation, and determination of the polarization plane and incidence angle need to be considered. The use of commercial photometers, with diverging beam configuration, can cause significant systematic errors.

Also a method that can be easily used to take into account the effects of dispersion during the data analysis by using the Nonlinear Schrödinger equation to model nonlinear phase shift and nonlinear coefficient is demonstrated. These improvements do not modify the basic idea of the direct continuous-wave self-phase modulation method, but are easy to implement in already existing measurement setups. The technique also allows flexible adjustment of the measured fiber length, wavelength spacing of the dual-frequency signal, fiber dispersion and launched optical power. It is also reasonable to expect that the same approach would improve the accuracies of other techniques used to measure the nonlinearity of optical fibers.

At the moment the determination of nonlinear coefficient n_2/A_{eff} of optical fibers is typically limited due to the optical power measurement. It is evident that high accuracy fiber optic detectors are needed to improve the level of uncertainty. A good solution for this problem is a fiber optic detector based on the integrating sphere and a mounted InGaAs photodiode. It is capable of measuring high optical power without any external attenuator and therefore offers better repeatability as the number of fiber connections is reduced. Among the fiber community, the issues related to the traceability of optical power measurements and uncertainty analysis need careful consideration, if better agreement between different laboratories and measurement methods is aimed at.

References

[1] H. J. Kostkowski, "Reliable Spectroradiometry", Spectroradiometry Consulting (1997).

[2] J. E. Martin, N. P. Fox and P. J. Key, "A cryogenic radiometer for absolute radiometric measurements", *Metrologia* **21**, 147-155 (1985).

[3] T. Varpula, H. Seppä and J.-M. Saari, "Optical power calibrator based on a stabilized green He-Ne laser and a cryogenic radiometer", *IEEE Trans. Instrum. Meas.* **28**, 558-564 (1989).

[4] T. R. Gentile, J. M. Houston and C. L. Cromer, "Realization of a scale of absolute spectral response using the National Institute of Standards and Technology high accuracy cryogenic radiometer", *Appl. Opt.* **35**, 4392-4403 (1996).

[5] E. Theocharous, T. R. Prior, P. R. Haycocks and N. P. Fox "High-accuracy, infrared, spectral responsivity scale", *Metrologia* **35**, 543-548 (1998).

[6] P.-S. Shaw, T. C.Larason, R. Gupta, S. W. Brown and K. R. Lykke "Improved Near-Infrared Spectral Responsivity Scale", *J. Res. Natl. Inst. Stand. Technol.* **105**, 689-700 (2000).

[7] L. Werner, R. Friedrich, U. Johannsen and A. Steiger, "Precise scale of spectral responsivity for InGaAs detectors based on a cryogenic radiometer and several laser sources", *Metrologia* **37**, 523-526 (2000).

[8] P.-S. Shaw, T. C. Larason, R. Gupta, S. W. Brown, R. E. Vest and K. R. Lykke "The new ultraviolet spectral responsivity scale based on cryogenic radiometry at Synchrotron Ultraviolet Radiation Facility III", *Rev. Sci. Instrum.* **72**, 2242-2247 (2001).

[9] J. Campos, A. Pons and P. Corredera, "Spectral responsivity scale in the visible range based on single silicon photodiodes", *Metrologia* **40**, S181–S184 (2003).

[10] Ö. Bazkir and F. Samadov, "Characterization of silicon photodiode-based trap detectors and establishment of spectral responsivity scale", *Opt. Lasers Eng.* **43**, 131-141 (2005).

[11] P. Meindl, A. E. Klinkmüller, L. Werner, U. Johannsen and K. Grützmacher, "New UV spectral responsivity scale of the PTB based on a cryogenic radiometer and an argon plasma arc radiation source", *Metrologia* **43**, S72–S77 (2006).

[12] E. F. Zalewski and C. R. Duda, "Silicon photodiode device with 100 % external quantum efficiency", *Appl. Opt.* **22**, 2867-2873 (1983).

[13] N. P. Fox, "Trap Detectors and their Properties", *Metrologia* **28**, 197-202 (1991).

[14] J-M. Coutin, F. Chandoul and J. Bastie, "GaAsP trap detector for UV measurement" in 6th Workshop on Ultraviolet Radiation Measurements, Davos, Switzerland, 20-21 October, 2005, Abstracts of Presentations, pp. 32-34, URL: http://metrology.hut.fi/uvnet/source/ws6abstr.pdf.

[15] K. Solt, H. Melchior, U. Kroth, P. Kuschnerus, V. Persch, H. Rabus, M. Richter and G. Ulm, "PtSi–n–Si Schottky-barrier photodetectors with stable spectral responsivity in the 120–250 nm spectral range", *Appl. Phys. Lett.* **69**, 3662-3664 (1996).

[16] P. Kuschnerus, H. Rabus, M. Richter, F. Scholze, L. Werner and G. Ulm, "Characterization of photodiodes as transfer detector standards in the 120 nm to 600 nm spectral range", *Metrologia* **35**, 355-362 (1998).

[17] K. D. Stock, R. Heine and H. Hofer, "Spectral characterization of Ge trap detectors and photodiodes used as transfer standards", *Metrologia* **40**, 163-166 (2003).

[18] K. D. Stock and R. Heine, "Spectral characterization of InGaAs trap detectors and photodiodes used as transfer standards", *Metrologia* **37**, 449-452 (2000).

[19] K. C. Kao and G. A. Hockman, "Dielectric fiber surface waveguides for optical frequencies", *Proc. IEE* **133**, 1151-1158 (1966).

[20] R. J. Mears, L. Reekie, I. M. Jauncey, D. N. Payne, "Low-noise erbium-doped fibre amplifier operating at 1.54 µm", *Electron. Lett.* **23**, 1026-1028 (1987)

[21] E. Desurvire, J. R. Simpson, P. C. Becker, "High-gain erbium-doped traveling-wave fiber amplifier", *Opt. Lett* **12**, 888-890 (1987).

[22] 0. E. Delange, "Wideband optical communication systems, Part II - Frequency division multiplexing", *Proc. IEEE* **58**, 1683 (1970).

[23] W. Tomlinson, "Wavelength multiplexing in multimode optical fibers", *Appl. Opt.* **18**, 2180-2194 (1977).

[24] D. Marcuse, A. R. Chraplyvy and R. W. Tkach, "Effect of Fiber Nonlinearity on Long-Distance Transmission", *J. Lightwave Technol.* **9**, 121-128 (1991).

[25] B. Batagelj, "Need of Knowing Fiber Non-linear Coefficient in Optical Networks", in *6th WSEAS International Conference on Communications*, Rethymno, Greece, (2002).

[26] G. P. Agrawal, "Nonlinear Fiber Optics", 3rd ed., Academic Press (2001).

[27] Bureau International des Poids et Mesures, "The International System of Units (SI)", 8th edition (2006).

[28] T. R. Gentile, J. M. Houston, J. E. Hardis, C. L. Cromer and A. C. Parr, "National Institute of Standards and Technology high-accuracy cryogenic radiometer", Appl. Opt. 35, 1056-1068 (1996).

[29] J. Ireland, M.G. White and N.P. Fox, "Cryogenic radiometer developments at NPL", in *9th International Conference on New Developments and Applications in Optical Radiometry*, Davos, Switzerland, Conference Proceedings, p. 39 (2005).

[30] Ö. Bazkir, S. Ugur, F. Samedov and A. Esendemir "High-accuracy optical power measurements by using electrical-substitution cryogenic radiometer", *Opt. Eng.* **44**, 016401 (2005).

[31] R. Köhler, R. Goebel, R. Pello, O. Touayar, J. Bastie, "First results of measurements with the BIPM cryogenic radiometer and comparison with the INM cryogenic radiometer", *Metrologia* **32**, 551-555 (1995).

[32] R. Goebel, R. Pello, R. Köhler,P. Haycocks, N. Fox, "Comparison of the BIPM cryogenic radiometer with a mechanically cooled cryogenic radiometer from the NPL", *Metrologia* **33**, 177-179 (1996).

[33] K. D. Stock, H. Hofer, J. G. S. Romero, L. P. G. Galván, W. Schmid, "Cryogenic radiometer facility of the CENAM and first international comparison", *Metrologia* **37**, 269-271 (2000).

[34] P. Kärhä, A. Haapalinna, P. Toivanen, F. Manoocheri and E. Ikonen, "Filter radiometry based on direct utilization of trap detectors", *Metrologia* **35**, 255-259 (1998).

[35] T. Kübarsepp, P. Kärhä, F. Manoocheri, S. Nevas, L. Ylianttila and E. Ikonen, "Spectral irradiance measurements of tungsten lamps with filter radiometers in the spectral range 290 nm to 900 nm", *Metrologia* **37**, 305-312 (2000).

[36] E. Ikonen, P. Toivanen, A. Lassila, "A new optical method for high-accuracy determination of aperture area", *Metrologia* **35**, 369-372 (1998).

[37] A. Haapalinna, F. Manoochehri and E. Ikonen, "High-accuracy measurement of specular spectral reflectance and transmittance", *Anal. Chim. Acta* **380**, 317-325 (1999).

[38] International Bureau of Weights and Measures, "Mutual recognition of national measurement standards and of calibration and measurement certificates issued by national metrology institutes", Paris, 14 October 1999, <http://kcdb.bipm.org/>.

[39] International Bureau of Weights and Measures, “The BIPM key comparison data base. Appendix C, Calibration and measurement capabilities of National Metrology Institutes”, http://kcdb.bipm.org_appendixC.

[40] R. Goebel, S. Yilmaz , R. Pello, “Polarization dependence of trap detectors”, *Metrologia* **33**, 207-213 (1996).

[41] J. M. Palmer, “Alternative Configurations for Trap Detectors”, *Metrologia* **30**, 327-333 (1993).

[42] J. L. Gardner, “Transmission trap detectors”, *Appl. Opt.* **33**, 5914-5918 (1994).

[43] T. Kübarsepp, P. Kärhä and E. Ikonen, “Characterization of a polarization-independent transmission trap detector”, *Appl. Opt.* **36**, 2807-2812 (1997)

[44] F. Manoocheri, P. Kärhä, L. Palva, P. Toivanen, A. Haapalinna and E. Ikonen, “Characterization of optical detectors using high-accuracy instruments”, *Anal. Chim. Acta* **380**, 327-337 (1999).

[45] L. P. Boivin, “Realization of Spectral Responsivity Scales” Optical Radiometry in Experimental Methods in the Physical Sciences, Optical Radiometry, Vol. 41, Elsevier Inc. (2005).

[46] W. C. Dash and R. Newman, “Intrinsic optical absorption in single-crystal germanium and silicon at 77°K and 300°K”, *Phys. Rev.* **99**, 1151-1155 (1955).

[47] H. R. Philipp and E. A. Taft, “Optical Constants of Germanium in the region 1 eV to 10 eV”, *Phys Rev.* **113**, 1002-1005 (1959).

[48] K. D. Stock, “Internal quantum efficiency of Ge photodiodes”, *Appl. Opt.* **27**, 12-14 (1998).

[49] P. Lecollinet and J. Bastie, “Fatigue effects in germanium photodetectors”, *Metrologia* **30**, 351-354 (1993).

[50] S. Nevas, F. Manoocheri and E. Ikonen, “Gonioreflectometer for measuring spectral diffuse reflectance”, *Appl. Opt.* **43**, 6391-6399 (2004).

[51] J.A. Dobrowolski, F.C. Ho and A. Waldorf, “Determination of optical constants of thin film coating materials based on inverse synthesis”, *Appl. Opt.* **22**, 3191-3200 (1983).

[52] E. D. Palik, “Handbook of optical constants of solids”, Academic Press, pp 465-478 (1985), ISBN 0-12-544420-6.

[53] G. P. Eppeldauer and R. J. Martin, “Photocurrent measurement of PC and PV HgCdTe Detectors”, *J. Res. Natl. Inst. Stand. Technol.* **106**, 577-587 (2001).

[54] G. Eppeldauer, “Electronic characteristics of Ge and InGaAs radiometers”, *SPIE Proceedings* **3061**, 833-838 (1997).

[55] K. D. Stock, R. Heine and H. Hofer, “Influence of inhomogeneity of NIR-photodiodes on calibrations at 1047 nm”, *Metrologia* **28**, 207-210 (1991).

[56] T. C. Larason and S S Bruce, “Spatial uniformity of responsivity for silicon, gallium nitride, germanium, and indium arsenide photodiodes”, *Metrologia* **35**, 491-496 (1998).

[57] T. M. Hunt, N. P. Fox, W. S. Hartree and N. M. Durant, “Evaluating the performance of filter radiometers as a means of improving the uncertainty of ultraviolet measurements”, *Metrologia* **35**, 345-351 (1998).

[58] T. Kübarsepp, P. Kärhä and E. Ikonen,” Interpolation of the Spectral Responsivity of Silicon Photodetectors in the Near Ultraviolet”, *Appl. Opt.* **39**, 9-15 (2000).

[59] T. Saito, K. Katori, M. Nishi, and H. Onuki, “Spectral quantum efficiencies of semiconductor photodiodes in the far ultraviolet region”, *Rev. Sci. Instrum.* **60**, 2303-2306 (1989).

[60] T. Saito, K. Katori, and H. Onuki, “Characteristics of semiconductor photodiodes in the VUV region”, *Phys. Scripta* **41**, 783-787 (1990).

[61] T. Saito, M. Yuri, and H. Onuki, “Polarization characteristics of semiconductor photodiodes”, *Metrologia* **32**, 485-489 (1995).

[62] K. Solt, H. Melchior, U. Kroth, P. Kuschnerus, V. Persch, H. Rabus, M. Richter and G. Ulm, “PtSi–*n*–Si Schottky-barrier photodetectors with stable spectral responsivity in the 120–250 nm spectral range”, *Appl. Phys. Lett.* **69**, 3662-3664 (1996).

[63] T. M. Hunt, N. P. Fox, W. S. Hartree and N. M. Durant, “Evaluating the performance of filter radiometers as a means of improving the uncertainty of ultraviolet measurements”, *Metrologia* **35**, 345-351 (1998).

[64] N. P. Fox, E. Theocharous and T. H. Ward, “Establishing a new ultraviolet and near-infrared spectral responsivity scale”, *Metrologia* **35**, 535-541 (1998).

[65] P. S. Shaw, K.R. Lykke, R. Gupta, T. R. O’Brian, U. Arp, H. H. White, T. B. Lucatorto, J. L. Dehmer and A. C. Parr, “Ultraviolet radiometry with synchrotron radiation and cryogenic radiometer“, *Appl. Opt.* **38**, 18-28 (1999).

[66] P. S. Shaw, T. C. Larason, R. Gupta, S. W. Brown, R. E. Vest and K. R. Lykke, “The new ultraviolet spectral responsivity scale based on cryogenic radiometry at Synchrotron Ultraviolet Radiation Facility III”, *Rev. Sci. Instrum.* **72**, 2242-2247 (2001).

[67] R. L. Gallawa and X. Li, “Calibration of optical fiber power meters: the effect of connectors”, *Appl. Opt.* **26**, 1170-1174 (1987)

[68] J. H. Lehman and X. Li, “A transfer standard for optical fiber power metrology”, *Eng. Lab. Notes in Opt. & Photon. News* **10**, *Appl. Opt.* **38**, 7164–7166 (1999).

[69] John H. Lehman and Christopher L. Cromer, “Optical trap detector for calibration of optical fiber powermeters: coupling efficiency”, *Appl. Opt.* **41**, 6531-6536 (2002).

[70] L.P. Boivin, “Properties of sphere radiometers suitable for high-accuracy cryogenic-radiometer-based calibrations in the near-infrared,” *Metrologia* **37**, 273-278 (2000).

[71] P. Corredera, J. Campos, M.L. Hernanz, J.L. Fontecha, A. Pons, and A. Corróns, “Calibration of near-infrared transfer standards at optical-fibre communication wavelengths by direct comparison with a cryogenic radiometer,” *Metrologia* **35**, 273-277 (1998).

[72] J. Envall, P. Kärhä and E. Ikonen, “Measurement of fibre optic power using photodiodes with and without an integrating sphere”, *Metrologia* **41**, 353-358 (2004).

[73] A. Carrasco-Sanz, F. Rodríguez-Barrios, P. Corredera, S. Martín-López, M. González-Herráez, and M.L. Hernanz, “An integrating sphere radiometer as a solution for high power calibrations in fibre optics,” *Metrologia* **43**, S145-S150 (2006).

[74] A. Carrasco-Sanz, S. Martín-López, P. Corredera, M. González-Herráez and M. L. Hernanz, “High-power and high-accuracy integrating sphere radiometer: design, characterization, and calibration”, *Appl. Opt.* **45**, 511-518 (2006).

[75] E. Hecht, “Optics”, 4th International Ed., Addison Wesley (2002).

[76] K. S. Kim, R. H. Stolen, W. A. Reed and K. W. Quoi, “Measurement of nonlinear index of silica-core and dispersion-shifted fibers”, *Opt. Lett.* **19**, 257-259 (1994).

[77] J. Envall, A. Andersson, J. C. Petersen and P. Kärhä, “Realization of the scale of high fiber optic power at three national standards laboratories”, *Appl. Opt.* **44**, 5013-5017 (2005).

[78] E. F. Zalewski and J. Geist, “Solar cell spectral response characterization”, *Appl. Opt.* **18**, 3942-3947 (1979).

[79] H. A. Macleod, “Thin-film optical filters”, 2nd Ed., Adam Hilger Ltd (1986).

[80] J. D. Rancourt, “Optical thin films user handbook”, SPIE – International Society for Optical Engineering (1996).

[81] Optilayer Ltd., “Advanced Thin Film Optical Coatings”, Chapter Evaluation and Design (2001).

[82] S. Nevas, “Characterization of materials and components using accurate spectrophotometric measurements and mathematical modeling”, Thesis for the degree of Doctor of Technology, Helsinki University of Technology, Espoo, Finland (2004).

[83] W. E. Case, “Algebraic method for extracting thin-film optical parameters from spectrophotometer measurements”, *Appl. Opt.* **22**, 1832-1836 (1983).

[84] R. C. McPhedran, L. C. Botten, D. R. McKenzie and R. P. Netterfield, “Unambiguous determination of optical constants of absorbing films by reflectance and transmittance measurements”, *Appl. Opt.* **23**, 1197-1205 (1984).

[85] L. Ward, “The accuracy of photometric methods for determination of optical constants of thin absorbing films,” J. Phys. D. 15, 1361-1371 (1982).

[86] L. Vriens and W. Rippens, “Optical constants of absorbing thin films on a substrate”, *Appl. Opt.* **22**, 4105-4110 (1983).

[87] A. H. M. Holtslag and P. M. L. O. Scholte, “Optical measurements of the refractive index, layer thickness, and volume changes of thin films”, *Appl. Opt.* **28**, 5095-5104 (1989).

[88] K. Lamprecht, W. Papousek and G. Leising, “Problem of ambiguity in the determination of optical constants of thin absorbing films from spectroscopic reflectance and transmittance measurements”, *Appl. Opt.* **36**, 6364-6371 (1997).

[89] T. Babeva, S. Kitova and I. Konstantinov, “Photometric methods for determining the optical constants and the thicknesses of thin absorbing films: selection of a combination of photometric quantities on the basis of error analysis”, *Appl. Opt.* **40**, 2675-2681 (2001).

[90] T. Babeva, S. Kitova and I. Konstantinov, “Photometric methods for determining the optical constants and the thicknesses of thin absorbing films: criteria for precise and unambiguous determination of *n*, *k*, and *d* in a wide spectral range,” *Appl. Opt.* **40**, 2682-2686 (2001).

[91] P. O. Nilsson, “Determination of optical constants from intensity measurements at normal incidence”, *Appl. Opt.* **7**, 435-442 (1968).

[92] R. K. Ahrenkiel, “Modified Kramers-Kronig analysis of optical spectra”, *J. Opt. Soc. Am.* **61**, 1651-1655 (1971).

[93] K. F. Palmer, M. Z. Williams, B. A. Budde, “Multiply Subtractive Kramers Kronig Analysis of Optical Data”, *Appl. Opt.* **37**, 2660-2673 (1998).

[94] I. Chambouleyron, J. M. Martínez, A. C. Moretti and M. Mulato, “Retrieval of optical constants and thicknesses of thin films from transmission spectra”, *Appl. Opt.* **31**, 8238-8247 (1997).

[95] M. Nenkov and T. Pencheva, “Calculation of thin-film optical constants by transmittance-spectra fitting”, *J. Opt. Soc. Am. A* **15**, 1852-1857 (1998).

[96] H. G. Tompkins and W. A. McGahan, “Spectroscopic Ellipsometry and Reflectometry”, John Wiley & Sons (1999).

[97] K. M. Gustin, “Optical characterization of low-index transparent thin films on transparent substrates by spectroscopic ellipsometry”, *Appl. Opt.* **26**, 3796-3802 (1987).

[98] K. Postava, M. Aoyama, T. Yamaguchi, and H. Oda, “Spectroellipsometric characterization of materials for multilayer coatings”, Appl. Surf. Sci. 175-176, 276-280 (2001).

[99] D. Bhattacharyya, N. K. Sahoo, S. Thakur, N. C. Das, “Characterization of a multilayer highly reflecting mirror by spectroscopic phase-modulated ellipsometry”, *Appl. Opt.* **40**, 1707-1714 (2001)

[100] J. C. Manifacier, J. Gasiot and J. P. Fillard, "A simple method for the determination of the optical constants *n*, *k* and the thickness of a weakly absorbing thin film", *J. Phys. E* **9**, 1002-1004 (1976).

[101] R. Swanepoel, "Determination of the thickness and the optical constants of amorphous silicon", *J. Phys. E* **16**, 1214-1222 (1983).

[102] I. Ohlídal, D. Franta, M. Ohlídal and K. Navrátil, "Optical characterization of nonabsorbing and weakly absorbing thin films with the wavelengths related to extrema in spectral reflectances", *Appl. Opt.* **40**, 5711-5717 (2001).

[103] A. V. Tikhonravov, M. K. Trubetskov, M. A. Kokarev, T. V. Amotchkina, A. Duparré, E. Quesnel, D. Ristau and S. Günster, "Effect of systematic errors in spectral photometric data on the accuracy of determination of optical parameters of dielectric thin films", *Appl. Opt.* **41**, 2555-2560 (2002).

[104] S. Nevas, F. Manoocheri and E.Ikonen, "Determination of thin film parameters from high accuracy measurements of spectral regular transmittance", *Metrologia* **40**, S200-S203 (2003).

[105] S. Nevas, F. Manoocheri, E. Ikonen, A. Tikhonravov, M. Kokarev and M. Trubetskov, "Optical metrology of thin films using high-accuracy spectrophotometric measurements with oblique angles of incidence", in Advances in Optical Thin Films, C. Amra, N. Kaiser, H. A. Macleod, eds., *Proc. SPIE* **5250**, 234-242 (2004).

[106] F. Manoochehri and E. Ikonen, "High-accuracy spectrometer for measurement of regular spectral transmittance", *Appl. Opt.* **34**, 3686-3692 (1995).

[107] International Telecommunication Union, "Definitions and test methods for statistical and non-linear attributes of single-mode fibre and cable," ITU-T Rec. G.650.2 (01/2005).

[108] R. Ramaswami and K. N. Sivarajan, "Optical Networks", 2nd ed., Academic Press (2002).

[109] A. Boskovic, S. V. Chernikov, J. R. Taylor, L. Gruner-Nielsen and O. A. Levring, "Direct continuous-wave measurement of n_2 in various types of telecommunication fiber at 1.55μm", *Opt. Lett.* **21**, 1966-1968 (1996).

[110] J.-C. Antona, S. Bigo and S. Kosmalski, "Nonlinear index measurements of various fibre types ovar C+L bands using four-wave mixing", in *27th European Conference on Optical Communication*, Amsterdam, The Netherlands, Conference Digest, pp. 270-271 (2001).

[111] K. Nakajima, T. Omae and M. Ohashi, "Conditions for measuring nonlinear refractive index n_2 of various single-mode fibres using cw-SPM method", *IEE Proc.-Optoelectron.* **148**, 209-214 (2001).

[112] T. Omae, K. Nakajima and M. Ohashi, "Universal Conditions for Estimating the Nonlinear Refractive Index n_2 of Dispersion-Compensating Fibers by the CW-SPM Method", *IEEE Photonics Technol. Lett*. **13**, 571-573 (2001).

[113] L. Prigent and J.-P. Hamaide, "Measurement of fiber nonlinear Kerr coefficient by four-wave mixing", *IEEE Photonics Technol. Lett.* **5**, 1092–1095 (1993).

[114] S. Song, C. T. Allen, K. R. Demarest and R. Hui, " Intensity-Dependent Phase-Matching Effects on Four-Wave Mixing in Optical Fibers", *J. Lightwave Technol.* **17**, 2285-2290 (1999).

[115] B. Batagelj and M. Vidmar, "Fiber Nonlinear coefficient measurement scheme based on Four-Wave Mixing method with externally modulated laser source", in *4th International Conference on Transparent Optical Networks*, Warsaw, Poland, Conference Digest, pp. 184-187 (2002).

[116] M. Tadakuma, O. Aso and S. Namiki, "Nonlinear coefficient measurement of reverse dispersion fiber using four-wave mixing", in *5th Optical Fibre Measurement Conference*, Nantes, France, Conference Digest, pp. 71-74 (1999).

[117] H. Chen, "Simultaneous measurements of non-linear coefficient, zero-dispersion wavelength and chromatic dispersion in dispersion-shifted fibers by four-wave mixing", *Opt. Commun.* **220**, 331-335 (2003).

[118] R. H. Stolen and C. Lin, "Self-phase-modulation in silica optical fibers", *Pys. Rev. A* **17**, 1448-1454 (1978).

[119] R. H. Stolen, W. A. Reed, K. S. Kim and G. T. Harvey, "Measurement of the Nonlinear Refractive index of Long Dispersion-Shifted Fibers by Self-Phase Modulation at 1.55 µm", *J. Lightwave Technol.* **16**, 1006-1012 (1998).

[120] M. Monerie and Y. Durteste, "Direct interferometric measurement of nonlinear refractive index of optical fibers by crossphase modulation", *Electron. Lett.* **23**, 961-963 (1987).

[121] T. Kato, Y. Suetsugu, M. Takagi, E. Sasaoka, and M. Nishimura, "Measurement of the nonlinear refractive index in optical fiber by cross-phase-modulation method with depolarized pump light", *Opt. Lett.* **20**, 988-990 (1995).

[122] M. Artiglia, E. Ciaramella and B. Sordo, "Using modulation instability to determine Kerr coefficient in optical fibres", *Electron. Lett.* **31**, 1012-1013 (1995).

[123] Y. Namihira, "ITU-T Round Robin Measurement for Nonlinear Coefficient (n_2/A_{eff}) of various Single Mode Optical Fibers", in *Symposium of Optical Fiber Measurements*, Boulder, Colorado, USA, NIST Special Publication 1024, pp. 33-36 (2004).

[124] L. Råde and B. Westergren, "Mathematics Handbook for Science and Engineering (BETA)", 4th ed., Studentlitteratur (1998).

[125] T. I. Lakoba and G. P. Agrawal, "Effects of third-order dispersion on dispersion-managed solitions", *J. Opt. Soc. Am. B* **16**, 1332-1343 (1999).

[126] Y. Namihira, M. Suzuki, R. S. Khera, S. V. Chernikov and J. R. Taylor, "Interlaboratory fiber nonlinear coefficient measurements for various dispersion shifted fibers at 1550nm", in *5th Optical Fibre Measurement Conference*, Nantes, France, Conference Digest, pp. 66-69 (1999).

[127] Y. Namihira, "KDD nonlinear coefficient round robin measurements for various dispersion shifted fibres in Japan and UK", in *Symposium of Optical Fiber Measurements*, Boulder, Colorado, USA, Conference proceedings, pp. 49-52 (2000).

[128] Y. Namihira, "Nonlinear coefficient round robin measurements for various dispersion shifted fibers in Japan and UK", in *26th European Conference on Optical Communication*, Munich, Germany, Conference proceedings, pp. 97-98 (2000).

[129] Y. Namihira and R. Alexander, "Interim report of ITU-T nonlinear coefficient (n_2/A_{eff}) round robin measurement results in Japan", in *6th Optical Fibre Measurement Conference*, 2001, Cambridge, UK, Conference Digest, pp.63-66 (2001).

[130] Y. Namihira, K. Miyagi, K. Kaneshima, M. Tadakuma, C. Vinegoni, G. Pietra and K. Kawanami, "A comparison of six techniques for nonlinear coefficient measurements of various single mode optical fibers", in *12th Symposium on Optical Fiber Measurement*, Boulder CO, USA, Technical Digest, pp. 15-18 (2002).

[131] Y. Namihira, "ITU-T nonlinear coefficient (n_2/A_{eff}) round robin measurements for various optical fibers in Japan, USA, Switzerland and Italy", in *29th European Conference on Optical Communication and 14th International Conference on Integrated Optics and Optical Fibre Communications*, Rimini, Italy, Conference proceedings, pp. 636-637 (2003).

[132] P. K. A. Wai, C. R. Menyuk and H. H. Chen, "Stability of solitons in randomly varying birefringent fibers", *Opt. Lett.* **16**, 1231-1233 (1991).

[133] S. G. Evangelides, Jr., L. F. Mollenauer, J. P. Gordon and N. S. Bergano, "Polarization multiplexing with solitons", *J. Lightwave Technol.* **10**, 28-35 (1992).

[134] S.V. Chernikov and J. R. Taylor, "Measurement of normalization factor of n_2 for random polarization in optical fibers", *Opt. Lett.* **21**, 1559-1561 (1996).

[135] ISO/IEC/OIML/BIPM, "Guide to the Expression of Uncertainty in Measurements", International Organization for Standardizations, Geneva, ISO/TAG 4/WG 3, June 1992.

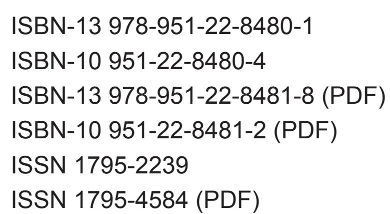

ISBN-13 978-951-22-8480-1
ISBN-10 951-22-8480-4
ISBN-13 978-951-22-8481-8 (PDF)
ISBN-10 951-22-8481-2 (PDF)
ISSN 1795-2239
ISSN 1795-4584 (PDF)